CHEMISTRY OF MATERIALS
Review

Chem. Mater. **2010,** *22,* 587–603 587
DOI:10.1021/cm901452z

Challenges for Rechargeable Li Batteries[†]

John B. Goodenough* and Youngsik Kim

Texas Materials Institute, University of Texas at Austin, Austin, Texas 78712

Received May 27, 2009. Revised Manuscript Received July 9, 2009

The challenges for further development of Li rechargeable batteries for electric vehicles are reviewed. Most important is safety, which requires development of a nonflammable electrolyte with either a larger window between its lowest unoccupied molecular orbital (LUMO) and highest occupied molecular orbital (HOMO) or a constituent (or additive) that can develop rapidly a solid/electrolyte-interface (SEI) layer to prevent plating of Li on a carbon anode during a fast charge of the battery. A high Li^+-ion conductivity ($\sigma_{Li} > 10^{-4}$ S/cm) in the electrolyte and across the electrode/electrolyte interface is needed for a power battery. Important also is an increase in the density of the stored energy, which is the product of the voltage and capacity of reversible Li insertion/extraction into/from the electrodes. It will be difficult to design a better anode than carbon, but carbon requires formation of an SEI layer, which involves an irreversible capacity loss. The design of a cathode composed of environmentally benign, low-cost materials that has its electrochemical potential μ_C well-matched to the HOMO of the electrolyte and allows access to two Li atoms per transition-metal cation would increase the energy density, but it is a daunting challenge. Two redox couples can be accessed where the cation redox couples are "pinned" at the top of the O 2p bands, but to take advantage of this possibility, it must be realized in a framework structure that can accept more than one Li atom per transition-metal cation. Moreover, such a situation represents an *intrinsic voltage limit* of the cathode, and matching this limit to the HOMO of the electrolyte requires the ability to tune the intrinsic voltage limit. Finally, the chemical compatibility in the battery must allow a long service life.

Introduction

It is now almost universally recognized that gaseous emissions from the burning of fossil fuels and biomass are not only polluting the air of large, modern cities but are also creating a global warming with alarming consequences. Moreover, a dependence on foreign oil and/or gas creates national vulnerabilities that endanger social stability. These concerns are concentrating attention once again on national initiatives to reevaluate utilization of alternative energy sources and replacement of the internal combustion engine with a wireless electric motor.

Solar radiation, wind, and waves represent energy sources that are variable in time and diffuse in space.[1] These sources require energy storage. Nuclear reactors provide a constant energy source with associated problems of radioactive waste disposal. Geothermal energy is restricted in location. These energy sources also benefit from electrical energy storage. The energy carriers are the electricity grid, electromagnetic waves, and chemical energy. The most convenient form of energy storage is portable chemical energy, which is the reason for our addiction to fossil fuels for heat, propulsion, lighting, and communication. The battery provides the portability of stored chemical energy with the ability to deliver this energy as electrical energy with a high conversion efficiency and no gaseous exhaust. Moreover, the alternative energy sources are preferably converted to d.c. electrical energy well-matched to storage as chemical energy in a battery. Whereas alternative energy sources are stationary, which allows other means of energy storage to be competitive with a battery, electric vehicles require the portable stored energy of a fuel fed to a fuel cell or of a battery. Therefore, of particular interest is a low-cost, safe, rechargeable (secondary) battery of high voltage, capacity, and rate capability.

The higher stored volume and gravimetric energy density of a Li battery has enabled realization of the cellular telephone and lap-top computer. However, cost, safety, stored energy density, charge/discharge rates, and service life are issues that continue to plague the development of the Li battery for the potential mass market of electric vehicles to alleviate distributed CO_2 emissions and noise pollution.[2]

A battery consists of a group of interconnected electrochemical cells. Here, we focus on batteries for electric vehicles where cost, gravimetric energy density, and the performance uniformity of individual cells in a large, multicell battery are of more concern than the volume energy density considered critical for hand-held appliances. Moreover, we consider only the choice of active materials in the individual cells of a secondary battery,

[†] Accepted as part of the 2010 "Materials Chemistry of Energy Conversion Special Issue".

*Author to whom correspondence should be directed. E-mail: jgoodenough@mail.utexas.edu.

Published on Web 08/28/2009

viz. the anode (negative electrode), the cathode (positive electrode), and the electrolyte between the electrodes.

Preliminary Considerations

Figure 1 is a schematic of the relative electron energies in the electrodes and the electrolyte of a thermodynamically stable battery cell having an aqueous electrolyte. The anode is the reductant, the cathode is the oxidant, and the energy separation E_g of the lowest unoccupied molecular orbital (LUMO) and the highest occupied molecular orbital (HOMO) of the electrolyte is the "window" of the electrolyte. The two electrodes are electronic conductors with anode and cathode electrochemical potentials μ_A and μ_C (their Fermi energies ε_F). An anode with a μ_A above the LUMO will reduce the electrolyte unless a passivation layer creates a barrier to electron transfer from the anode to the electrolyte LUMO; a cathode with a μ_C below the HOMO will oxidize the electrolyte unless a passivation layer blocks electron transfer from the electrolyte HOMO to the cathode. Therefore, thermodynamic stability requires locating the electrode electrochemical potentials μ_A and μ_C within the window of the electrolyte, which constrains the open-circuit voltage V_{oc} of a battery cell to

$$eV_{oc} = \mu_A - \mu_C \leq E_g \qquad (1)$$

where e is the magnitude of the electron charge. A passivating solid/electrolyte-interface (SEI) layer at the electrode/electrolyte boundary can give a kinetic stability to a larger V_{oc} provided that $eV_{oc} - E_g$ is not too large.

On discharge, electrons leave the anode via an external circuit where they do useful work before entering the cathode. To retain charge neutrality in the electrodes, cations are released from the anode to the electrolyte and the working cation of the electrolyte, the H^+ ion in an aqueous electrolyte, carries positive charge to the cathode to provide charge neutrality in the cathode. The process is reversed on charge in a rechargeable (secondary) battery.

The energy density of a battery cell is ΛV_{oc}; Λ is the capacity of reversible charge transfer per unit weight (Ah/g) between the anode and cathode. Λ decreases with the rate of charge or discharge, i.e. the magnitude of the electronic current in the external circuit, which must be matched by the internal ionic current within the battery. Since the ionic current density of the electrolyte and electrodes, including the rate of ion transfer across the electrode/electrolyte interface, is much smaller than the electronic current density, the electrodes and electrolyte have a large surface area and a small thickness. Nevertheless, at high current densities, the ionic motion within an electrode and/or across an electrode/electrolyte interface is too slow for the charge distribution to reach equilibrium, which is why the reversible capacity decreases with increasing current density in the battery and why this capacity loss is recovered on reducing the rate of charge and/or discharge.

The high H^+-ion conductivity required of an aqueous electrolyte over the practical ambient-temperature range

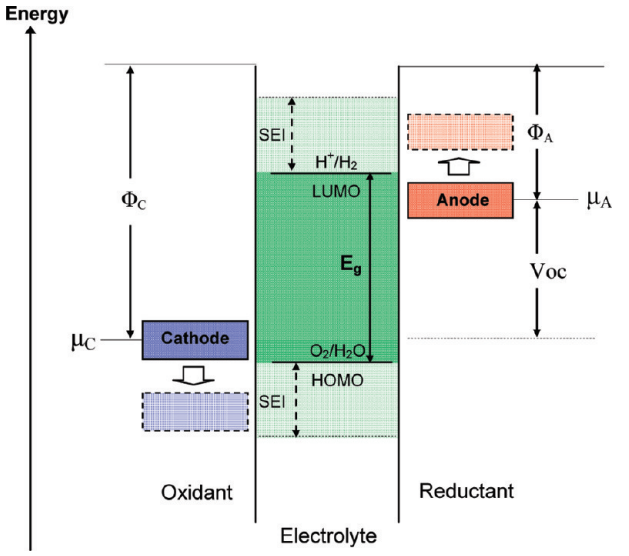

Figure 1. Schematic open-circuit energy diagram of an aqueous electrolyte. Φ_A and Φ_C are the anode and cathode work functions. E_g is the window of the electrolyte for thermodynamic stability. A $\mu_A >$ LUMO and/or a $\mu_C <$ HOMO requires a kinetic stability by the formation of an SEI layer.

is only found in liquid or immobilized-liquid water, and an $E_g \approx 1.3$ eV for an aqueous electrolyte limits V_{oc}. In order to obtain a cell with a higher V_{oc} and therefore a higher energy density ΛV_{oc}, it is necessary to turn to a nonaqueous electrolyte with a larger E_g. This observation, in turn, has led to the Li^+-ion battery since lithium salts are soluble in some nonaqueous liquids and polymers. However, in this case, the HOMO of the salt as well as that of the solvent may determine the limiting μ_C of the cathode.

Once the window of the Li^+-ion electrolyte has been determined, it is necessary to design electrodes of high capacity that have their μ_A and μ_C matched to the LUMO and HOMO of the electrolyte. Elemental Li^0 would be the ideal anode, but the $\varepsilon_F = \mu_A$ of Li^0 lies above the LUMO of practical, known nonaqueous electrolytes. Therefore, use of Li^0 as an anode is only possible because a passivating SEI layer is formed. The SEI layer allows use of Li^0 as an anode in half-cells used to obtain the μ_A or μ_C of a practical electrode relative to the Li^+/Li^0 energy level; but on repeated charge/discharge cycles, breaking of the SEI layer in selected areas results in the formation of dendrites that can grow across the electrolyte to short-circuit a cell of the battery with dangerous consequences. Therefore, we must design either (1) an anode with a μ_A matched to the LUMO of the electrolyte as well as a cathode with a μ_C matched to the HOMO of the electrolyte or (2) a stable passivating SEI layer that self-heals rapidly when broken by the changes in electrode volume that occur in a charge/discharge cycle; the SEI layer must also permit a fast Li^+-ion transfer between the electrode and the electrolyte without blocking electron transfer between the active particle and the current collector.

In summary, the formidable challenges for the developer of a rechargeable Li battery for the potential mass market of electric vehicles are three-fold: to identify

Table 1. Nonaqueous Electrolytes for Li-Ion Batteries

Electrolytes	Example of classical electrolytes	Ionic conductivity ($\times 10^{-3}$ s/cm) at room temp	Electrochemical window (V) vs Li^+/Li^0		Remark
			Reduction	Oxidation	
Liquid organic	1M $LiPF_6$ in EC:DEC (1:1)	7[3]	1.3[7]	4.5[6]	Flammable
	1M $LiPF_6$ in EC:DMC (1:1)	10[3]	1.3[7]	> 5.0[3]	
Ionic liquids	1M LiTFSI in EMI-TFSI	2.0[15]	1.0[15]	5.3[15]	Non-flammable
	1M $LiBF_4$ in EMI-BF_4	8.0[15]	0.9[16]	5.3[16]	
Polymer	LiTFSI-P(EO/MEEGE)	0.1[24]	< 0.0[24]	4.7[24]	Flammable
	$LiClO_4$−PEO_8 + 10 wt % TiO_2	0.02[26]	< 0.0[26]	5.0[26]	
Inorganic solid	$Li_{4-x}Ge_{1-x}P_xS_4$ (x = 0.75)	2.2[28]	< 0.0[28]	> 5.0[28]	Non-flammable
	0.05Li_4SiO_4 + 0.57Li_2S + 0.38SiS_2	1.0[30]	< 0.0[30]	> 8.0[30]	
Inorganic liquid	$LiAlCl_4$ + SO_2	70[20]	-	4.4[20]	Non-flammable
Liquid organic + Polymer	0.04$LiPF_6$ + 0.2EC + 0.62DMC + 0.14PAN	4.2[38]	-	4.4[38]	Flammable
	$LiClO_4$ + EC + PC + PVdF	3.0[39]	-	5.0[39]	
Ionic liquid + Polymer	1M LiTFSI + P_{13}TFSI + PVdF-HFP	0.18[43]	< 0.0[43]	5.8[43]	Less flammable
Ionic liquid + Polymer + Liquid organic	56 wt % LiTFSI−Py_{24}TFSI + 30 wt % PVdF-HFP + 14 wt % EC/PC	0.81[44]	1.5[44]	4.2 [44]	Less flammable
Polymer + Inorganic solid	2 vol % $LiClO_4$-TEC-19 + 98 vol% 95 (0.6Li_2S + 0.4Li_2S) + 5Li_4SiO_4	0.03[46]	< 0.0[46]	> 4.5[46]	Non-flammable
Ionic liquid + Liquid organic[19]		-	-	-	Non-flammable

low-cost, environmentally benign materials for the three active components of a battery cell, viz. (1) a nonaqueous electrolyte of high Li^+-ion conductivity ($\sigma_{Li} > 10^{-3}$ S/cm) over the practical ambient-temperature range $-40 < T < 60$ °C that has a window allowing a thermodynamically stable $V_{oc} \geq 4$ V and (2) an anode and (3) a cathode with their μ_A and μ_C values well-matched to the window of the electrolyte as well as each allowing a fast charge/discharge cycle of large reversible capacity.

Electrolytes

In addition to a large electrolyte window E_g, the electrolyte must satisfy several additional requirements such as:

1) Retention of the electrode/electrolyte interface during cycling when the electrode particles are changing their volume.
2) A Li^+-ion conductivity $\sigma_{Li} > 10^{-4}$ S/cm over the temperature range of battery operation.
3) An electronic conductivity $\sigma_e < 10^{-10}$ S/cm.
4) A transference number $\sigma_{Li}/\sigma_{total} \approx 1$, where σ_{total} includes conductivities by other ions in the electrolyte as well as $\sigma_{Li} + \sigma_e$.
5) Chemical stability over ambient temperature ranges and temperatures in the battery under high power.
6) Chemical stability with respect to the electrodes, including the ability to form rapidly a passivating solid/electrolyte-interface (SEI) layer where kinetic stability is required because the electrode potential lies outside the electrolyte window.
7) Safe materials, i.e., preferably nonflammable and nonexplosive if short-circuited.
8) Low toxicity and low cost.

Meeting all these requirements proves to be a formidable challenge.

Types of Electrolytes. In general, the electrolyte is specifically designed for a particular battery application. Table 1 shows several different materials that have been used as electrolytes for Li batteries.

Organic Liquid Electrolytes. Carbonates are organic liquids that are reasonably good solvents for Li salts.[3,4] They have an oxidation potential (HOMO) at ca. 4.7 V[3,5,6] and a reduction potential (LUMO) near 1.0 V.[7] (All voltages in this paper are referred to the Li^+/Li^0 potential.) Moreover, they have a relatively low viscosity, which results in a low activation energy for Li^+-ion diffusion. Therefore, the most commonly used electrolytes are carbonates or carbonate blends consisting of one or more of the following: propylene carbonate (PC), ethylene carbonate (EC), diethyl carbonate (DEC), dimethyl carbonate (DMC), or ethylmethyl carbonate (EMC). In order to be able to use carbon as the anode, which has its electrochemical potential above (at a lower voltage versus Li^+/Li^0) that of the LUMO of a carbonate, the solvents include, in most cases, ethylene carbonate (EC) because the EC provides a passivating

solid/electrolyte-interface (SEI) layer on the surface of a carbon anode that protects the electrolytes from further decomposition after SEI formation.[8,9] However, carbonate-based solvents are highly flammable with flash points below 30 °C.[10] In addition, the preferred salt, $LiPF_6$, can undergo an autocatalytic decomposition into LiF and PF_5; the PF_5 reacts irreversibly with any water present ($PF_5 + H_2O = PF_3O + 2HF$) and, above 60 °C, with a carbonate electrolyte.[11] These reactions degrade the battery and lead to safety hazards. However, additives used to lower the operating temperature have been shown to prevent the autocatalytic decomposition of $LiPF_6$ salt.[12]

Ionic Liquids. Room-temperature ionic liquids (RTILs)[13−17] have been recently considered as alternative electrolytes for Li-ion batteries because they offer several advantages over carbonate-based electrolytes: a high oxidation potential (~5.3 V vs Li^+/Li^0), nonflammability, a low vapor pressure, better thermal stability, low toxicity, high boiling points, and a high Li-salt solubility. Unfortunately, they have a higher viscosity, which reduces their Li^+-ion conductivity. Ionic liquids based on imidazolium-based cations would appear to be the most appropriate candidates for Li batteries due to their lower viscosity and a high Li-salt solubility at room temperature. However, these ionic liquids have poor stability at voltages below 1.1 V,[18] so that additives such as EC or VC must be added to introduce a stable SEI layer on a carbon anode. An alternative approach is to increase σ_{Li} by adding a liquid carbonate to an ionic liquid, but at a concentration that retains the nonflammability of the ionic liquid.[19] With this strategy, it is also possible to increase the oxidation voltage (lower HOMO energy) of the hybrid electrolyte from that of the carbonate. In spite of extensive research, no RTILs have yet been introduced into large power batteries.

Inorganic Liquid Electrolytes. The inorganic liquid electrolyte based on $LiAlCl_4$ and SO_2 proposed by Stassen and Hambitzer[20,21] has a good room-temperature $\sigma_{Li} = 7 \times 10^{-2}$ S/cm and is nonflammable, but its electrolyte window appears to be too small to be competitive.

Solid Polymer Electrolytes. A solid electrolyte can act as the separator of the electrodes, and a solid polymer electrolyte can also retain contact over an electrode/electrolyte interface during modest changes of the electrode volume with the state of charge of the battery. Polyethylene oxides (PEOs) containing a lithium salt ($LiPF_6$ or $LiAsF_6$)[22−24] are low-cost, nontoxic, Li^+-ion polymer electrolytes with good chemical stability, but the Li^+-ion conductivity, $\sigma_{Li} < 10^{-5}$ S/cm at room temperature, is too low for a power-battery system. The introduction of oxide particles (e.g., Al_2O_3, TiO_2, SiO_2, or ZrO_2)[25−27] creates a more amorphous polymer matrix by inhibiting chain crystallization and attracting Li^+ from its salt. The result is an enhanced σ_{Li} and Li-ion transference number, but σ_{Li} is still not comparable to that of the carbonate electrolytes.

Inorganic Solid Electrolytes. Inorganic solid Li^+-ion conducting materials having a $\sigma_{Li} > 10^{-4}$ S/cm[28−31] have been considered for Li-based electrolytes, as has been extensively reviewed,[32] because they have a wide electrochemical window and additionally meet the electrolyte requirements from 2 to 7, not 1. For these reasons, laboratory-size all-solid-state Li-ion batteries have been investigated.[33−35] However, the first of the additional electrolyte requirements has excluded inorganic solid Li^+-ion electrolytes from consideration for large-scale batteries having solid electrodes. They have only been used in thin-film battery applications.[36]

Hybrid Electrolyte System. Hybrid electrolytes are blends of organic liquid electrolytes, ionic liquids, polymer electrolytes, and/or inorganic solid electrolytes:

Polymer + organic liquid (polymer gel)[37−40]
Ionic liquid + polymer electrolyte (ionic liquid polymer gel)[41−45]
Ionic liquid + polymer electrolyte + liquid organic electrolyte[43,44]
Ionic liquid + liquid organic electrolyte[19]
Polymer electrolyte + inorganic solid electrolyte[46−48]

The mixtures of two or more electrolytes are investigated in attempts to exploit the advantages of each constituent, but the disadvantages of each also appear. For example, the ionic conductivity is increased in the polymer gel electrolytes, but they are still flammable and have the irreversible capacity loss below 1 V associated with formation of a passivation layer.[40]

Electrode−Electrolyte Compatibility. Although thermodynamic stability of the electrolyte vis à vis the electrodes is possible where the μ_A and μ_C of the electrodes lie within the window of the electrolyte, nevertheless chemical reactions between the electrode and the electrolyte may occur. For example, the reversible electrochemical intercalation of Li into Li_xVS_2 was originally frustrated by use of the electrolyte $LiClO_4$ in PC,[49] but the electrolyte $LiPF_6$ in EC/DEC allows full electrochemical cycling between $LiVS_2$ and VS_2.[50]

The cathode spinel $Li_{1-x}[Mn_2]O_4$ provides another type of electrode−electrolyte reaction; an electrode surface disproportionation reaction $2Mn^{3+} = Mn^{2+} + Mn^{4+}$ results in dissolution of the Mn^{2+} from the electrode into the electrolyte.[51] This reaction, unless suppressed, gives an irreversible capacity loss of the cathode and migration of the Mn^{2+} across the electrolyte to the anode during charge to block Li^+-ion insertion into the anode. The result is an intolerable limitation of the service life of the cell.

In addition to chemical stability vis à vis the electrodes and higher temperatures, the electrolyte should not be decomposed by an anode μ_A at a higher energy than the electrolyte LUMO or a cathode μ_C at a lower energy than the HOMO. However, if μ_A or μ_C lie outside the window of the electrolyte, kinetic stability may be achieved by formation of a passivating SEI layer on the surface of the electrode, but at the expense of the loss in capacity to form the layer. Moreover, during a fast charge, the concentration of Li^+ ions may build up on the surface of the SEI layer, and where a change in volume of the electrode

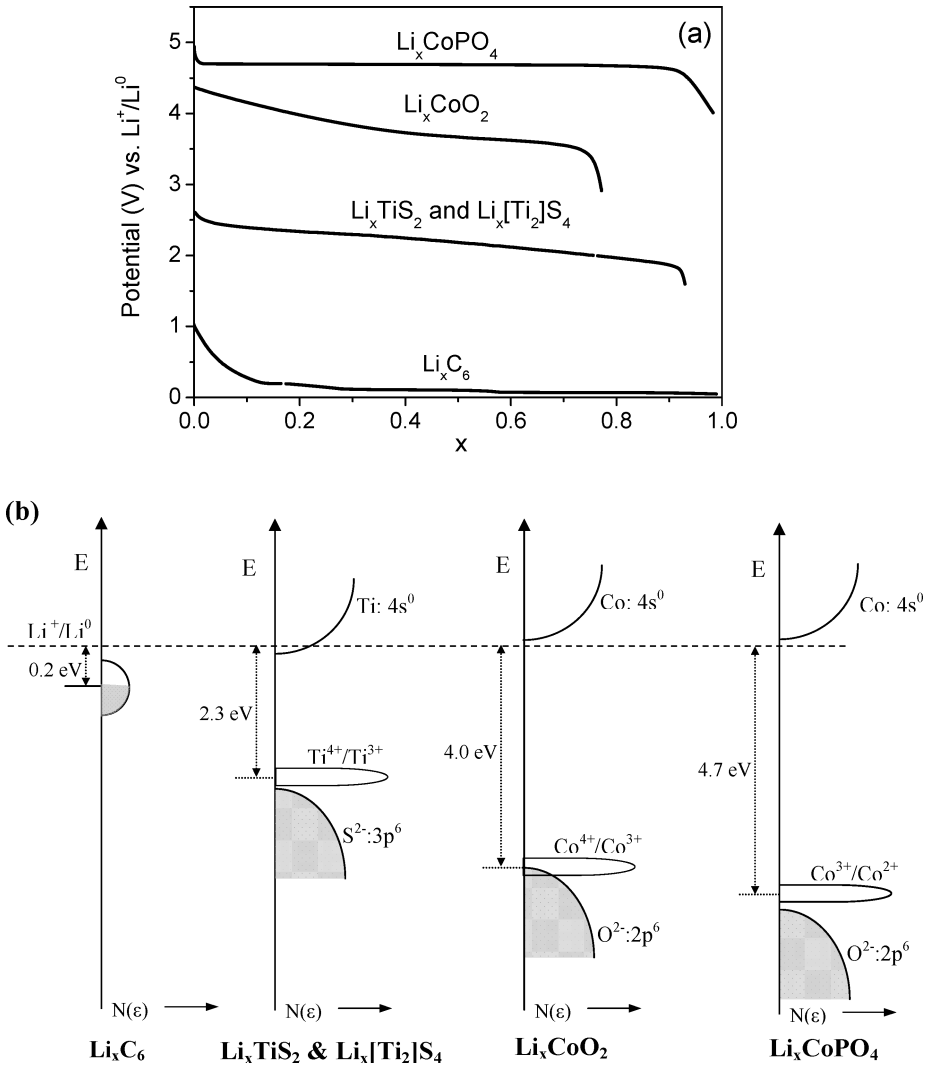

Figure 2. (a) Voltage profiles versus Li^+/Li^0 of the discharge curves of Li_xC_6, Li_xTiS_2 and $Li_x[Ti_2]S_4$, Li_xCoO_2, and Li_xCoPO_4. (b) Schematic of their corresponding energy vs density of states showing the relative positions of the Fermi energy in an itinerant electron band for Li_xC_6, the Ti^{4+}/Ti^{3+} redox couple for Li_xTiS_2 and $Li_x[Ti_2]S_4$, the Co^{4+}/Co^{3+} redox couple for Li_xCoO_2, and the Co^{3+}/Co^{2+} redox couple for Li_xCoPO_4.

breaks the SEI layer, Li^0 may be plated out before the break is healed. Li plating can result in dendrites that grow across the electrolyte. This problem creates a safety issue that has haunted the use of a carbon anode in large-scale power batteries. These problems need to be managed if safety standards are to be met with any anode, including carbon, that has its μ_A above the LUMO of the electrolyte.

A cathode μ_C at a lower energy than the electrolyte HOMO must be distinguished from an intrinsic voltage limit of the cathode, as is discussed below. As with anodes, passivating layers on cathodes are best formed *in situ* so that electronic contact with the cathode current collector is not broken. Preliminary work[52−54] on passivating SEI layers on oxide cathodes has found them to be unstable. This field has yet to be adequately researched.

Electrodes

The design of an electrode involves tailoring of the μ_A of an anode or μ_C of a cathode to the LUMO or HOMO of the Li^+-ion electrolyte to be used; the electrode must also be chemically stable in the electrolyte. To date, practical electrodes have all had host structures into/from which guest Li atoms can be inserted/extracted reversibly.

Factors Determining μ_A and μ_C. The energy of a given μ_A or μ_C may correspond to the Fermi energy in an itinerant-electron band, as is the case for carbon, or the energy of a redox couple of a transition-metal cation. Tailoring of the energy of a redox couple depends not only on the formal valence state of the cation, but also on the covalent component of its nearest-neighbor bonding, which is influenced by the placement and character of any counter cations and by the Madelung energy of the ionic component of the bonding, which is influenced by the structure. In addition, the position of a redox couple relative to the bottom of a broad conduction band or to the top of an anion p band may determine the intrinsic voltage limit versus Li^+/Li^0 of a given electrode. This problem arises for a μ_C where the active redox couple is "pinned" at the top of the anion p bands. Pinning of redox couples and the intrinsic voltage limit are concepts described below. However, we first demonstrate in Figure 2 the range of voltages that are exhibited by host structures

into/from which Li^+ ions have been inserted reversibly. Carbon, Li_xTiS_2, and Li_xCoO_2 are all layered compounds, the $[Ti_2]S_4$ spinel host of $Li_x[Ti_2]S_4$ is strongly bonded in 3D, and Li_xCoPO_4 shows the influence of the countercation of the $(PO_4)^{3-}$ polyanion on the Co^{3+}/Co^{2+} couple relative to the Co^{4+}/Co^{3+} couple in the layered Li_xCoO_2 (charges on ions represent formal valence states, not actual charges). The upper voltage limits in the sulfides are much lower than those in the oxides. In Figure 3, we also show how the Mn^{4+}/Mn^{3+} couple of $Li_x[Mn_2]O_2$ in a spinel framework is shifted by more than 1 eV where the Li^+ ions change their position from octahedral to tetrahedral sites as $2 > x > 1$ decreases to $1 > x > 0$. The influence of structure is exemplified by the comparison in Figure 4 of the voltages from the Fe^{3+}/Fe^{2+} couple in the olivine Li_xFePO_4, the NASICON structure of $Li_{3+x}Fe_2(PO_4)_3$, and some diphosphates.[55]

Host Structures. The sulfur atoms of TiS_2 form a close-packed hexagonal array with Ti occupying alternate (001) planes of octahedral sites. The $TiS_{6/3}$ sheets of edge-shared octahedra are held together by van der Waals forces. Steele[56] originally suggested that intercalation of Li into the empty octahedral sites between the $TiS_{6/3}$ sheets would be reversible, which made TiS_2 a potential cathode for a rechargeable Li battery. Whittingham[57] was the first to demonstrate fast, reversible Li insertion into TiS_2 over the solid-solution range $0 \le x \le 1$ of Li_xTiS_2. However, attempts to make a TiS_2/Li^0 battery failed because dendrite formation on the Li^0 anode caused explosive failure. Nevertheless, these early experiments demonstrated that compounds into which Li can be inserted/extracted reversibly are candidate electrodes for the rechargeable Li battery.

The horizontal, dashed lines of Figure 5 are the energies relative to the Li^+/Li^0 potential of the LUMO and HOMO of the EC/DEC solvent containing the more benign $LiPF_6$ as the Li^+-ion salt. This figure shows that the energy μ_C of the Ti^{4+}/Ti^{3+} redox couple of Li_xTiS_2 is not well-matched to the HOMO of this electrolyte. Realization that TiS_2 approaches the voltage limit versus Li^+/Li^0 of a layered sulfide suggested exploration of Li insertion into layered oxides.[58] However, layered oxides are only found where a transition-metal cation forms an M=O bond as with the vanadyl V=O and molybdyl Mo=O cations of V_2O_5 and MoO_3.[59,60] On the other hand, $LiMO_2$ oxides forming an ordered rock-salt structure with Li and transition-metal M atoms on alternate (111) octahedral-site planes invited investigation of reversible Li extraction.[58,61] Removal of Li from ordered $LiMO_2$ allows operating on an M^{4+}/M^{3+} couple of lower energy than the Ti^{4+}/Ti^{3+} couple of TiS_2. However, removal of Li leaves a metastable compound, and M cations stable in tetrahedral sites either move into the partially occupied Li layer or transform the structure to spinel on removal of half of the Li. Moreover, good order of the Li and M atoms in the initial $LiMO_2$ is required. Nevertheless, removal of half of the Li from well-ordered $LiCoO_2$ at a $\mu_C \approx 4.0$ V versus Li^+/Li^0 for the Co^{4+}/Co^{3+} couple proved stable. This couple has a good match to the HOMO of the $LiPF_6$ in EC/DEC electrolyte, but only one Li for two cobalt represents a reduced capacity; and Co is too expensive and toxic for a large-battery mass market.

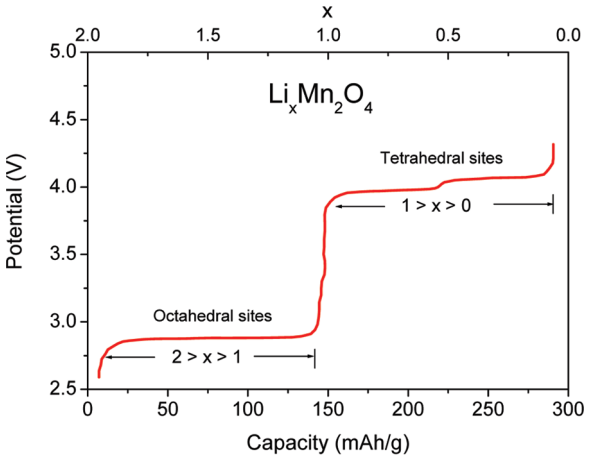

Figure 3. Voltage profile versus Li^+/Li^0 of the spinel $Li_xMn_2O_4$ ($2 \ge x \ge 0$). The Li^+ ions are shifted cooperatively from the tetrahedral to the octahedral sites as x increases though $x = 1$. Adapted from ref 67.

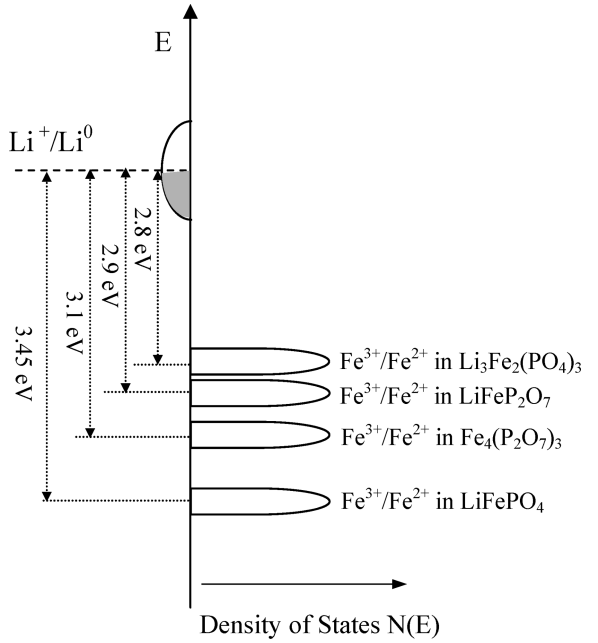

Figure 4. Positions of the Fe^{3+}/Fe^{2+} redox couples relative to the Fermi energy of lithium in different phosphates. Reprinted with permission from ref 55. Copyright 1997 The University of Texas at Austin.

Graphite has a layered structure that seemed to offer an intercalation anode to replace Li^0, but early attempts to use graphite were frustrated by reduction of the electrolyte on Li insertion.[62] As is shown in Figure 5, the μ_A of carbon lies well above the LUMO of a carbonate electrolyte, which is why identification of a Li intercalation compound is not a sufficient condition for a viable electrode. On the other hand, incorporation of ethylene carbonate (EC) into the carbonate electrolyte promotes formation of an SEI layer on the carbon that provides a kinetic stability.[8] An irreversible capacity loss on the

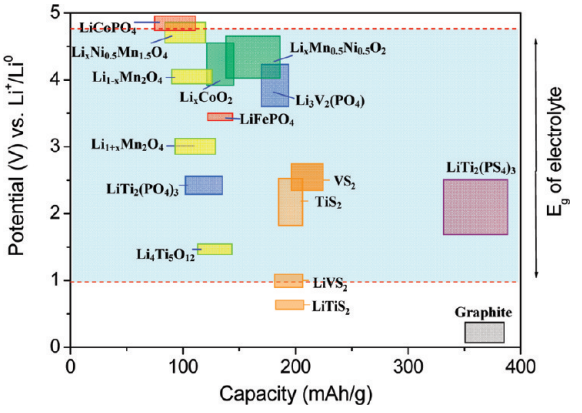

Figure 5. Voltage versus capacity of several electrode materials relative to the window of the electrolyte 1 M $LiPF_6$ in EC/DEC (1:1).

initial charge of the carbon anode is associated with the formation of a thin, amorphous SEI layer on the carbon that stabilizes reversible Li insertion/extraction on subsequent charge/discharge cycles, see Figure 6, with a reversible capacity of 370 mA h/g. Disordered carbon rather than graphitic carbon provides a better capacity.[63] With a passivated carbon anode and $LiCoO_2$ as the cathode, members of the Sony corporation launched the hand-held wireless revolution with their introduction of the wireless telephone.[64]

The next step was to recognize that framework structures offer strong 3D bonding as well as interstitial space for the insertion of Li^+ ions. For example, the $A[B_2]X_4$ spinels contain B cations in octahedral sites and A cations in tetrahedral sites of a close-packed-cubic X-atom array. The B cations are ordered to give a 3D-bonded $[B_2]X_4$ framework in which the interstitial space is interconnected by edge-sharing octahedral sites that share faces with the tetrahedral A sites; see Figure 7. Murphy and colleagues [65] removed Cu from $Cu[Ti_2]S_4$ and then inserted Li into the $[Ti_2]S_4$ spinel framework. In this sulfide, Li^+ ions initially enter the octahedral sites of the interstitial space rather than the tetrahedral sites, so the voltage versus x profile of $Li_x[Ti_2]S_4$, $0 \le x \le 1$, was essentially identical to that of the layered Li_xTiS_2.[57] Independent work at Oxford[66] showed that Li can be inserted into the oxospinels; but in oxides the Li species occupy the tetrahedral sites in $Li_{1-x}[B_2]O_4$. On insertion of Li into $Li[B_2]O_4$, Coulomb interactions between the Li^+ ions displace all the Li^+ ions to the octahedral sites. In the spinel $Li[Mn_2]O_4$, the high-spin Mn^{3+} ions are Jahn–Teller ions, and cooperative orbital ordering for a ratio $Mn^{3+}/Mn^{4+} > 0.5$ distorts the cubic structure to tetragonal to give a coexistence of two phases rather than a solid solution and therefore a flat $V_{oc} \approx 3.0$ V for $Li_{1+x}[Mn_2]O_4$. Subsequently, Thackeray et al.[67] showed that on removal of the Li from the tetrahedral sites of $Li_{1-x}[Mn_2]O_4$, the V_{oc} versus x profile was at 4.0 V versus Li^+/Li^0 for the same Mn^{4+}/Mn^{3+} redox couple. These observations, summarized in Figure 3, showed that shifting the Li^+ ions from octahedral to tetrahedral sites produces a 1 eV step in the Mn^{4+}/Mn^{3+} redox couple as a result of the inductive effect of the Li^+ ions. However, it also shows

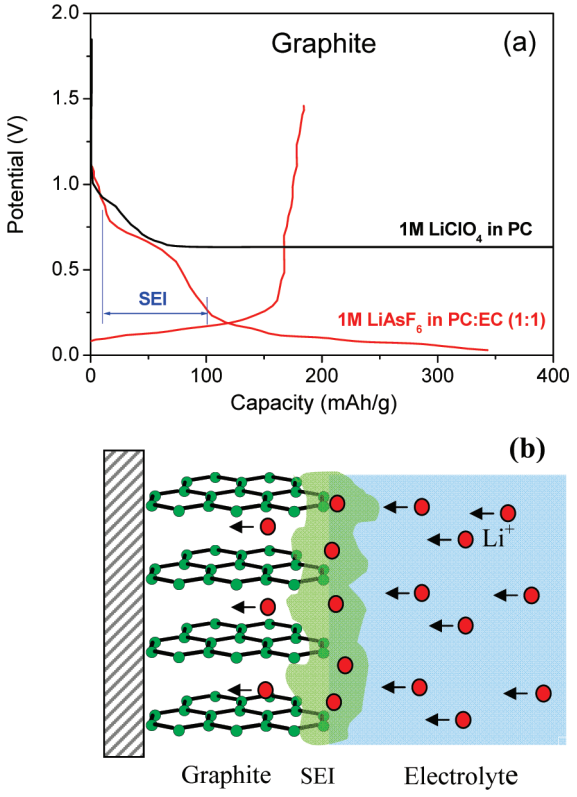

Figure 6. (a) Voltage curves of graphite tested in 1 M $LiClO_4$ in PC and 1 M $LiAsF_6$ in PC:EC (1:1) electrolytes. The electrolyte is reduced at $V \approx 0.7$ V in 1 M $LiClO_4$ in PC. An SEI layer is formed in the EC-based electrolyte between 0.8 and 0.4 V versus Li^+/Li^0, which allows further intercalation of Li^+ ions after an initial capacity loss. Adapted from refs 62 and 8. (b) Schematic presentation of the formation of the SEI layer by decomposition of EC-based electrolytes. Adapted from ref 9.

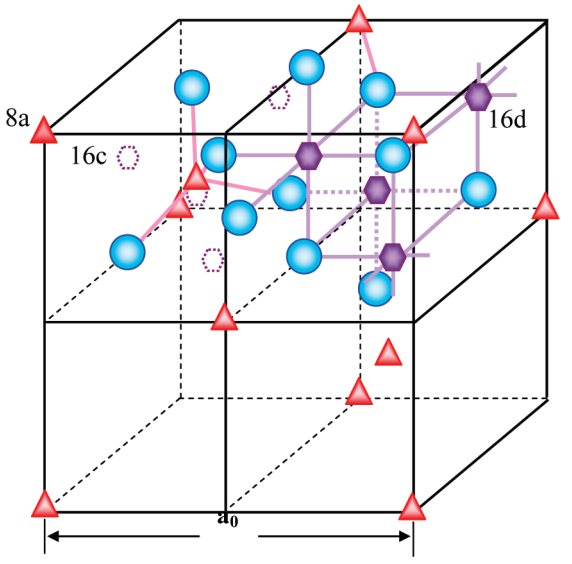

Figure 7. Two quadrants of the cubic spinel $A[B_2]X_4$ showing the occupied tetrahedral sites (8a), occupied octahedral sites (16d), and unoccupied octahedral sites (16c). The Li species of $Li_{1-x}[B_2]O_4$ occupy 8a tetrahedral sites, and those of $Li_{1+x}[B_2]O_4$ occupy only unoccupied octahedral sites (16c). The Li species of $Li_x[Ti_2]S_4$ occupy only unoccupied octahedral sites (16c) for all x of $0 \le x \le 2$. Adapted from ref 77.

that use of the oxospinels limits the operative capacity to one Li per two B-site cations as in layered $LiCoO_2$. Although Mn is cheaper and environmentally more

benign than Co, it has proven necessary to substitute some Li and Ni for Mn to suppress Li order at $Li_{0.5}[Mn_2]O_4$ and dissolution of Mn to the electrolyte on repeated charge/discharge cycling; the resulting further loss of capacity is only partially regained by the ability to replace some oxygen with fluorine.[68,69]

Another 3D framework is the $M_2(XO_4)_3$ structure of hexagonal $Fe_2(SO_4)_3$, which consists of clusters of two MO_6 octahedra bridged by three corner-sharing (XO_4) tetrahedra; the octahedra of these clusters share corners with the tetrahedra of neighboring clusters to create an open 3D host structure capable of accepting up to 5 Li atoms per formula unit into its interstitial space; see Figure 8. This framework is referred to as the NASICON structure since $Na_{1+3x}Zr_2(P_{1-x}Si_xO_4)_3$ was shown[70] to support fast Na^+-ion conduction, i.e. to be a *NA*-ion *S*uperior *I*onic *CON*ductor. Substitution of an (XO_4) polyanion for oxygen opens the host framework. Moreover, the observation[71] of a 0.6 V increase in the V_{oc} from $Li_{3+x}Fe_2(MoO_4)_3$ to $Li_{3+x}Fe_2(SO_4)_3$, each operating on the Fe^{3+}/Fe^{2+} couple, demonstrated that significant tuning of the energy of a redox couple can also be achieved through the inductive effect by changing the countercation in the polyanion. With this framework, it was possible to determine the relative energies of several redox couples in an oxide, Figure 9, and how these shift together on replacing (PO_4) with (SO_4).[72,73]

This exploration led to identification[74] of the olivine framework, Figure 10, of $FePO_4$ in which insertion of Li into its 1D channels gives a flat $V_{oc} = 3.45$ V versus Li^+/Li^0 for Li_xFePO_4, $0 \leq x \leq 1$, as a result of a small

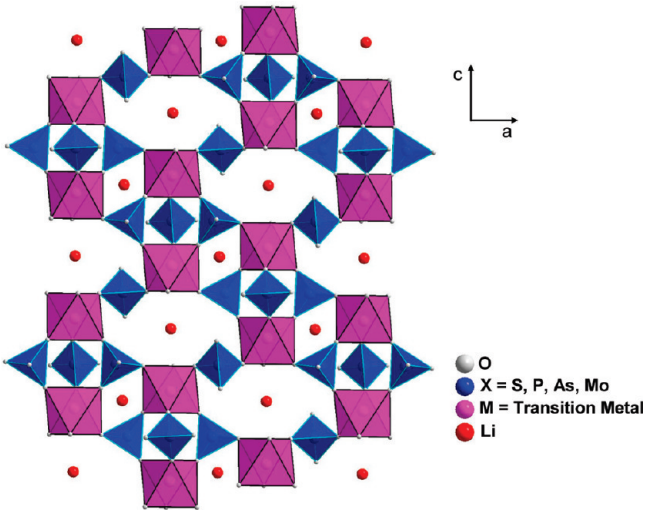

Figure 8. NASICON framework of $Li_xM_2(XO_4)_3$ that is built with MO_6 octahedra linked by corners to XO_4 tetrahedra and vice versa. Adapted from ref 70.

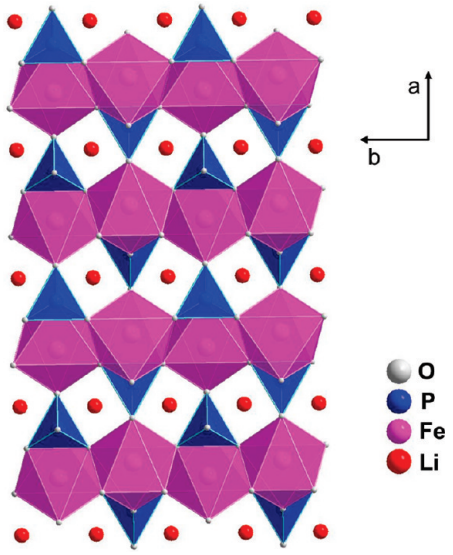

Figure 10. Olivine structure of $LiFePO_4$ showing Li in 1D channels. Adapted from ref 74.

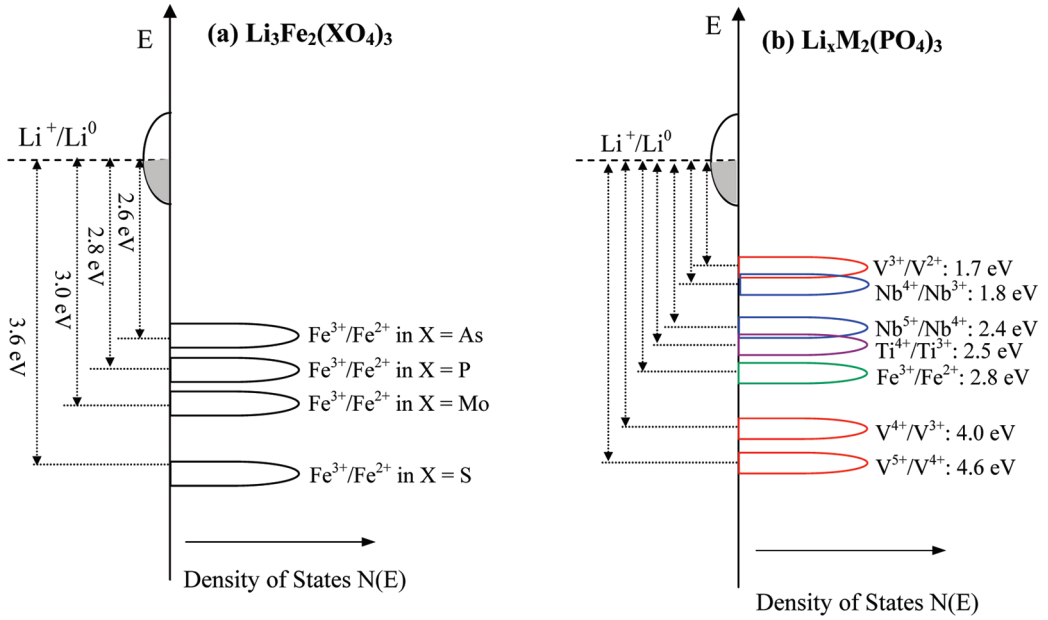

Figure 9. (a) Positions of the Fe^{3+}/Fe^{2+} redox couples relative to the Fermi energy of lithium in the NASICON structure with different polyanion countercations. Adapted from ref 55. (b) Positions of some M^n/M^{n+1} redox couples in $Li_xM_2(PO_4)_3$. Adapted from ref 73.

displacive structural change of the framework between $LiFePO_4$ and $FePO_4$. Despite the two-phase character for $0 < x < 1$, which results in a poor electronic conductivity, and the 1D channels for the Li motion, small particles of carbon-coated C−Li_xFePO_4 result in safe cathodes with reversible capacities that do not fade significantly on cycling thousands of times. However, the V_{oc} is not optimal for the $LiPF_6$ in the EC/DEC electrolyte. Nevertheless, a cell voltage $V_{oc} \approx 3$ V can be obtained with $LiFePO_4$ as a cathode and a carbon anode, which is excellent for many applications. However, to ensure safety for large-scale power applications, it would be preferable to have an anode with a $\mu_A \approx 1.3$ V versus Li^+/Li^0 if $LiPF_6$ in EC/DEC is used as the electrolyte. Such an anode with a $LiFePO_4$ cathode would, however, only give a cell $V_{oc} \approx 2$ V, which might not be competitive with a nickel/metal-hydride battery having an aqueous electrolyte.

Johnston[75] had shown that the spinel $Li[Ti_2]O_4$ is a superconductor and the system $Li[Li_xTi_{2-x}]O_4$, $0 \le x \le 1/3$, had been well-characterized,[76,77] but the identification of $Li_{1+x}[Li_{0.33}Ti_{1.67}]O_4$ as a potential anode with a flat $V_{oc} = 1.5$ V versus Li^+/Li^0 was first made by Ferg et al.[78] Although $Li_4Ti_5O_{12}$ represents a thermodynamically stable anode having no passivation layer, it has only a modest capacity and its use as an anode requires identification of a cathode with a better match to the HOMO of the electrolyte than $LiFePO_4$.

Intrinsic Voltage Limits. Pinning of a redox couple at the top of an anion p band provides an intrinsic voltage limit for a cathode.[79] Pinning occurs where, as is illustrated in Figure 11, the energy of a redox couple crosses the top of the anion p bands. At this crossover, the electronic states of a d^n redox couple change from primarily cation d, i.e. $(d + p)^n$, to primarily anion p, i.e. $(p + d)^n$ character, and where the couple has a primarily anion p character, the cation will appear to be in a lower valence state, d^{n+1} after oxidation of the couple. Nevertheless, the antibonding $(p + d)^n$ orbitals retain a d orbital symmetry and behave as a redox couple. However, as the percentage of anion p character increases as the redox couple falls further below the top of the anion p bands or with increasing oxidation beyond a critical value, the antibonding character of the states at the top of the anion p bands fades and holes occupy bonding anion p states; for larger concentrations of purely anion p holes, the holes become trapped in dianion antibonding states, e.g. $(S_2)^{2-}$ or $(O_2)^{2-}$.

The Co^{4+}/Co^{3+} and Ni^{4+}/Ni^{3+} redox couples in the layered oxides $Li_{1-x}CoO_2$ and $Li_{1-x}NiO_2$ are pinned at the top of the O 2p bands. The system $Li_{1-x}CoO_2$ shows a flat $V_{oc} \approx 4.0$ V versus Li^+/Li^0 for $0 < x \le 0.5$ because there is a coexistence of a polaronic, high-spin Co^{4+} in a low-x phase[80] and an itinerant-electron, low-spin Co^{4+}/Co^{3+} phase near $x = 0.5$. For $x > 0.5$, peroxide formation at the surface leads to a loss of O_2 by the surface reaction

$$2(O_2)^{2-} = 2O^{2-} + O_2\uparrow \qquad (2)$$

A $V_{oc} \approx 4.0$ V is the *intrinsic upper voltage limit* for $Li_{1-x}CoO_2$. Decomposition of the compound occurs at higher voltages.

The low-spin $Co_x^{4+}Co_{1-x}^{3+}$:$\pi^{*6-x}\sigma^{*0}$ redox couple of $Li_{1-x}CoO_2$ contains holes in the antibonding, itinerant π^* orbitals of t orbital parentage; the low-spin $Ni_x^{4+}Ni_{1-x}^{3+}$:$t^6\sigma^{*1-x}$ couple of $Li_{1-x}NiO_2$ contains electrons in the antibonding σ^* orbitals of e orbital parentage, and for $x > 0.6$ in $Li_{1-x}NiO_2$, holes become trapped in peroxide ions. The initial voltage with the σ^* orbitals is a little lower, at $V \approx 3.8$ V in layered $Li_{1-x}NiO_2$, which is why a greater concentration of Ni^{4+} valence is found before O_2 evolution than with Co^{4+} in $Li_{1-x}CoO_2$. It is the cubic ligand-field splitting of the octahedral-site 3d orbitals that raises the Ni^{4+}/Ni^{3+} couple above that of the low-spin Co^{4+}/Co^{3+} couple. Substitution of half of the Ni by Mn in $Li(Ni_{0.5}Mn_{0.5})O_2$ gives the formal valence states Ni^{2+} and Mn^{4+}. The Mn^{5+}/Mn^{4+} couple lies well-below the top of

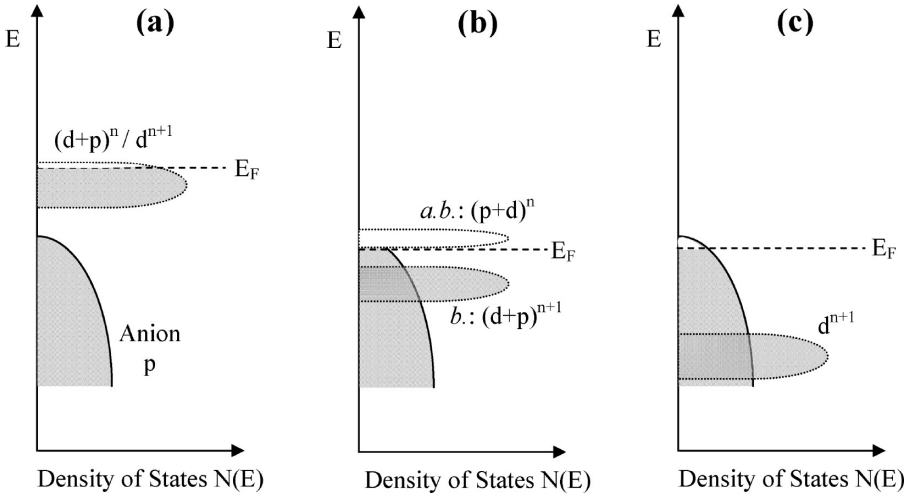

Figure 11. Schematic representation of a slightly oxidized redox couple for different positions relative to the top of the anion p bands. (a) Itinerant versus polaronic character of hole states of a couple on the approach to the top of the anion p band, (b) pinned couple with predominantly antibonding (*a.b.*) anion p hole states and predominantly cation d bonding (*b.*) states, and (c) couple too far below top of anion p band for significant cation d character in hole states. Reprinted with permission from ref 79. Copyright 2009 Elsevier.

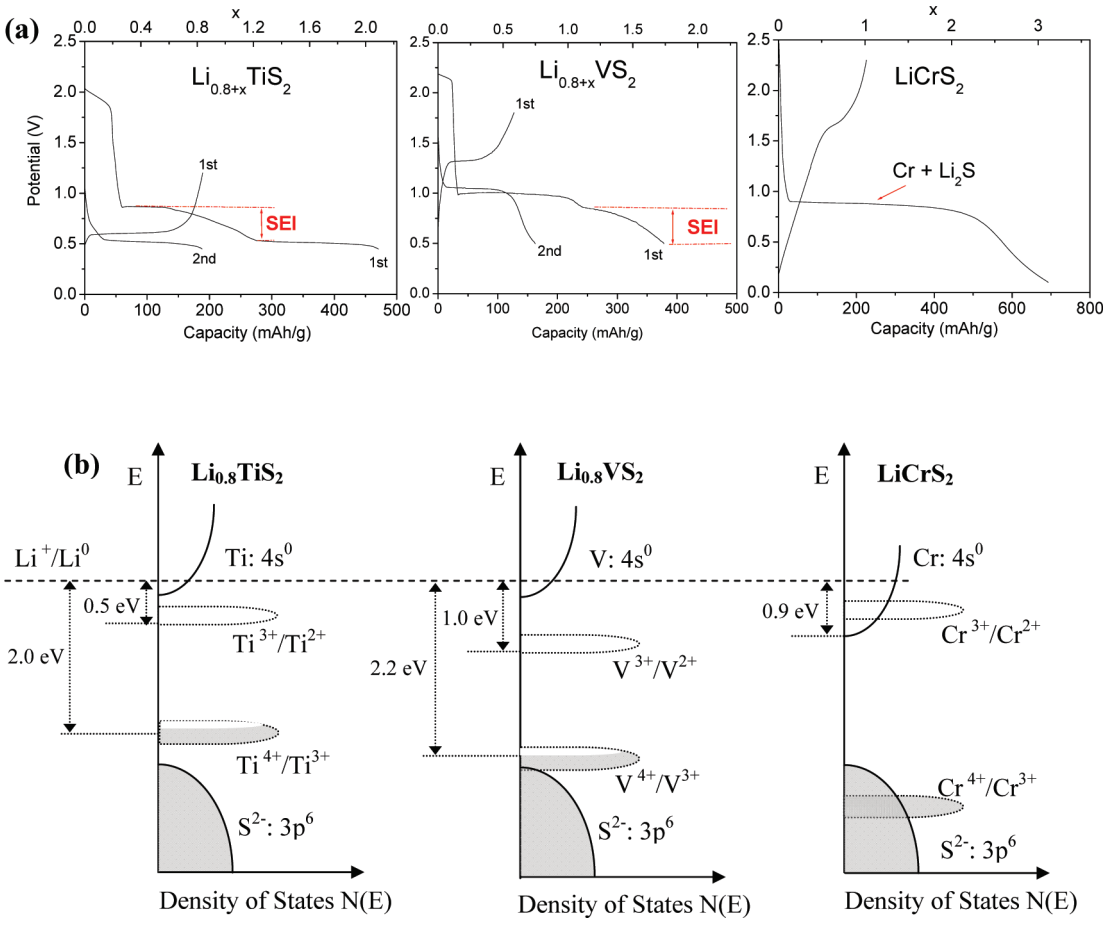

Figure 12. (a) Voltage profile for the discharge and charge curves on Li intercalation into $Li_{0.8}TiS_2$, $Li_{0.8}VS_2$, and $LiCrS_2$ tested in the 1 M $LiPF_6$ in EC:DEC (1:1) electrolyte. (b) Corresponding positions of the bottom of the 4s band, the top of the S 3p band, the M^{3+}/M^{2+}, and the M^{4+}/M^{3+} redox couples relative to the Fermi energy of lithium. Adapted from ref 82.

the O 2p bands, but the Ni^{3+}/Ni^{2+} couple is pinned at the top of the O 2p bands. In $Li_{1-x}(Ni_{0.5}Mn_{0.5})O_2$, the holes occupy a σ^* band of e^{2-2x} parentage at the Ni:$t^6\sigma^{*2-2x}$, so there is no step in the Fermi energy E_F on passing from the Ni^{3+}/Ni^{2+} to the Ni^{4+}/Ni^{3+} couple. Moreover, the Mn−Ni interaction raises the Ni^{4+}/Ni^{3+} redox couple relative to the top of the O 2p bands to give access to the entire Ni^{4+}/Ni^{3+} couple. Nevertheless, σ^* orbitals of $(e + p)^{2-2x}$ parentage change to $(p + e)^{2-2x}$ parentage as x increases.

The limiting lower voltage of an anode occurs where a redox couple crosses the bottom of the broad cation conduction band; e.g. the 4s band for the first-row transition-metal atoms. This situation is illustrated by Li insertion into the layered $LiMS_2$ sheets to create a coexistence of $LiMS_2$ and Li_2MS_2 phases and therefore a flat V versus x profile. The bottom of the M 4s band of the monosulfides MS lowers progressively as the M atom nuclear charge increases from M = Ti to M = Ni.[81] In $LiTiS_2$ and $LiVS_2$, the bottom of the 4s band is at ca. 0.15 eV below the Li^+/Li^0 Fermi energy; it is only a little lower at 0.85 eV in $LiCrS_2$.[82] As is evident in Figure 12, an SEI layer was formed rapidly on $Li_{0.8+x}MS_2$ (M = Ti, V) in the voltage range $0.5 < V < 0.9$ V versus Li^+/Li^0 on the first discharge; the Ti^{3+}/Ti^{2+} and V^{3+}/V^{2+} couples gave, respectively, a $V \approx 0.5$ and 1.0 V versus Li^+/Li^0. However, insertion of Li into $LiCrS_2$ yielded, in addition to the SEI layer, $Cr^0 + Li_2S$ at 0.85 V. The crystal-field splitting of the 3d orbitals lifts the σ-bonding e orbitals of high-spin Cr^{2+}:t^3e^1 above the bottom of the 4s band in $LiCrS_2$ even though CrS has been obtained chemically by Jellinek.[83] Since overlap of the S 3p orbitals with the Cr 4s is larger than with the Cr 3d orbitals, the covalent component of the Cr−S bond lifts the bottom of the 4s band of CrS above the energy of the $3d^4$ configuration to allow access to the Cr^{2+} valence state. In $Li_{1+x}CrS_2$, the sulfur atoms bond to Cr on one side and to Li on the other. Moreover, the Li species are forced into tetrahedral sites in Li_2CrS_2, and failure to access Cr^{2+} implies that a strong covalent component of the tetrahedral-site Li−S bond is reducing the covalent component in the Cr−S bond to leave the bottom of the Cr 4s band below the $3d^4$ energy. This observation illustrates how the bonding of a countercation can, through the inductive effect, change the *intrinsic limiting lower voltage* associated with a transition-metal cation.

Effect of Cation Substitutions. A countercation can, through the inductive effect, not only change an intrinsic limiting voltage associated with a transition-metal cation but also be used to tune the energy of an operative redox couple. This tuning phenomenon is illustrated in Figure 5 by comparison of the voltages associated with

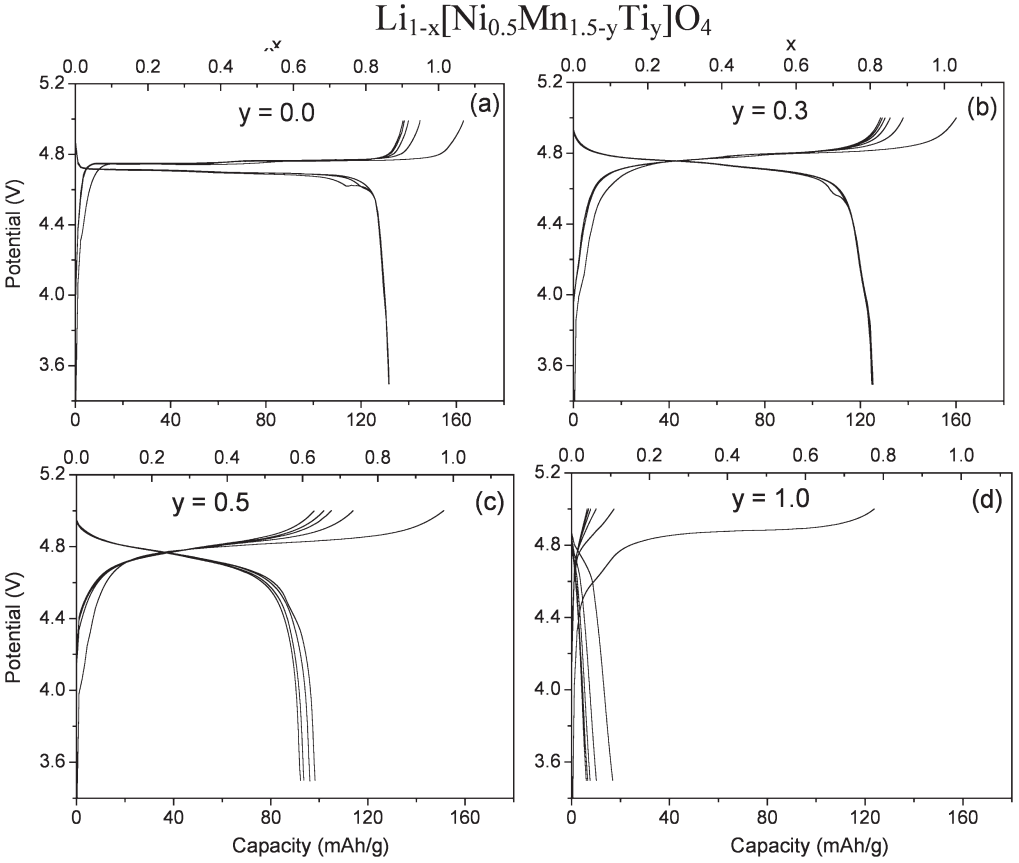

Figure 13. Voltage profiles of $Li_{1-x}[Ni_{0.5}Mn_{1.5-y}Ti_y]O_4$: (a) $y = 0$, (b) $y = 0.3$, (c) $y = 0.5$, and (d) $y = 1$. The capacity decreases and the voltage increases with higher Ti content. Adapted from ref 84.

the Ti^{4+}/Ti^{3+} couples in the NASICON framework of $Li_{1+x}Ti_2(PO_4)_3$ and the spinel $Li_4Ti_5O_{12}$. A change from 2.5 to 1.5 V shows that the countercation can have a profound effect on a redox energy through the inductive effect. Moreover, comparison of the Ni^{4+}/Ni^{3+} redox energy in layered $LiNiO_2$ where incomplete access is found at 3.8 V with that in the spinel $Li_{1-x}[Ni_{0.5}Mn_{1.5}]O_4$ where complete access is found at 4.75 V, see Figure 13a, shows that covalent bonding with the countercation can also increase the intrinsic limiting voltage of a cathode by lowering the top of the O 2p bands. We now inquire about the effect of cation substitution for the active cation on the intrinsic limiting voltage where the parent-cation redox energy is pinned at the top of an anion p band. For this purpose, we compare the influence of Mn^{4+} versus Ti^{4+} substitutions on the energies of the Ni^{3+}/Ni^{2+} and Ni^{4+}/Ni^{3+} couples in layered and spinel oxides. Comparison with the influence of Cr^{3+} substitutions for vanadium in the layered $LiV_{1-y}Cr_yS_2$ sulfides is also instructive.

Removal of Li from the tetrahedral sites of the spinel $Li_{1-x}[Ni_{0.5}Mn_{1.5}]O_4$ initially probes the Ni^{3+}/Ni^{2+} and then the Ni^{4+}/Ni^{3+} redox couples pinned at the top of the O 2p bands. Figure 13a shows that the voltage increases gradually with x from about 4.74 to 4.77 V in the first charge curve. The irreversible capacity loss in the first cycle corresponds to the formation of an SEI layer by the oxidation of the electrolyte. The irreversible capacity loss on each cycle is not characteristic of formation of a stable SEI layer; it represents oxidation of the electrolyte and an unstable SEI layer. Since the Ni^{4+}/Ni^{3+} couple of $LiNiO_2$ gives an initial voltage of 3.8 V, we may expect a voltage of 4.8 V versus Li^+/Li^0 for extraction of Li from the tetrahedral sites of the spinel if the top of the O 2p band and the pinned Ni^{4+}/Ni^{3+} couple are both stabilized by the shift of the Li^+ ions from octahedral to tetrahedral sites. Although the presence of the Mn^{4+} ions raises the Ni^{4+}/Ni^{3+} redox energy relative to the top of the O 2p bands, the voltage exceeds the HOMO of the electrolyte at about 4.75 V before the full Ni^{4+}/Ni^{3+} couple is accessed. In the spinel, the limitation is the HOMO of the electrolyte; it is not the intrinsic voltage limit of the cathode.

Figures 13b–d show what happens to the voltage profile as Mn is replaced by Ti in $Li[Ni_{0.5}Mn_{1.5-y}Ti_y]O_4$.[84] The octahedral-site Mn^{5+}/Mn^{4+} couple appears to be close enough to the top of the O 2p bands to be nearly pinned; the Mn^{5+} ion is stable in tetrahedral sites with a basic countercation. Interaction between the Mn^{5+}/Mn^{4+} and Ni^{4+}/Ni^{3+} pinned couples allows access to antibonding states at the top of the O 2p bands corresponding to a formal Ni^{4+}/Ni^{3+} couple. Missing this interaction, the Ni^{4+}/Ni^{3+} and Ni^{3+}/Ni^{2+} redox couples fall below the top of the O 2p band. As a result, the voltage increases with increasing Ti content in $Li[Ni_{0.5}Mn_{1.5-y}Ti_y]O_4$. However, the irreversible capacity loss is bigger with increasing Ti content and at higher Ti content ($y \geq 1.0$) insertion of Li does not permit access to even the

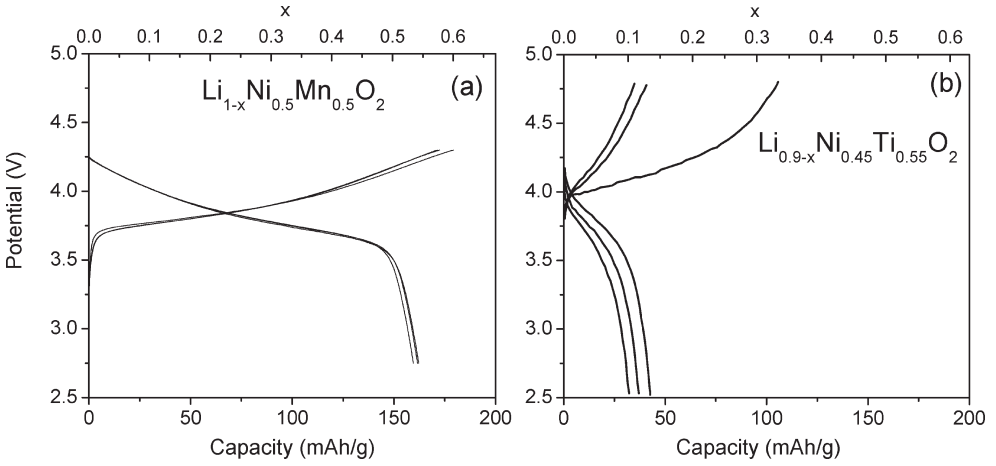

Figure 14. Voltage profiles of $Li_{1-x}[Ni_{0.5}Mn_{0.5}]O_2$ and $Li_{0.9-x}[Ni_{0.45}Ti_{0.55}]O_2$. Adapted from refs 85 and 86.

Ni^{3+}/Ni^{2+} redox couple; there appears a large irreversible curve at 4.9 V at $y = 1.0$. This is due to the fact that the two nickel redox couples fall further below the top of the O 2p bands with increasing Ti content in $Li[Ni_{0.5}Mn_{1.5-y}Ti_y]O_4$. Hence, the irreversible flat curve at 4.9 V corresponds to the irreversible access to the top of the O 2p bands, which indicates the intrinsic voltage limit of the spinel oxides. However, this can be confused with the oxidation potential of the electrolytes; it is estimated around 4.75 V.

Figure 14 compares the voltage profiles of the layered oxides $Li_{1-x}(Ni_{0.5}Mn_{0.5})O_2$[85] and $Li_{0.9-x}(Ni_{0.45}Ti_{0.55})O_2$.[86] In these examples, the voltages are well below the 4.75 V of the HOMO of the electrolyte. The Mn^{4+} raises the energies of the two nickel couples relative to the top of the O 2p bands, so the Ni^{4+} valence state is accessed reversibly. On the other hand, the Ti^{4+} apparently lowers the Ni^{3+}/Ni^{2+} couple relative to the top of the O 2p bands sufficiently to limit the intrinsic voltage of the layered oxide to under 4.0 V. Even the Ni^{3+}/Ni^{2+} couple is not completely accessed in the presence of Ti^{4+}.

Figure 15 compares the voltage profiles of layered oxides initially containing Ni^{2+} in the presence of Mn^{4+} with layered sulfides initially containing V^{3+} in the presence of Cr^{3+}. In the oxides, the Ni^{3+}/Ni^{2+} and Ni^{4+}/Ni^{3+} couples are pinned at the top of the O 2p bands; in the sulfides, the V^{4+}/V^{3+} and V^{5+}/V^{4+} couples are pinned at the top of the S 3p bands. Pinning of the redox couples of nickel gives an initial $V \approx 3.7$ V for $Li_{1-x}(Ni_{0.5}Mn_{0.5})O_2$, which is similar to the 3.8 V found[61] for the Ni^{4+}/Ni^{3+} couple of $Li_{1-x}NiO_2$. There is no step in the voltage profile at $x = 0.5$ where the Fermi energy falls from the Ni^{3+}/Ni^{2+} to the Ni^{4+}/Ni^{3+} couple. This lack of a step is a result of the pinning of the couples and the itinerant character of the holes. It is to be contrasted with the steps found, for example, in the NASICON structure,[87] as is illustrated in Figure 16. Finally, as already noted, the Ni^{4+} valence state is accessed without the evolution of O_2 because of the presence of Mn^{4+}. Similarly, $Li_{1-x}(V_{0.5}Cr_{0.5})S_2$ shows a reversible charge/discharge profile that varies smoothly through $x = 0.5$ because the V^{4+}/V^{3+} and V^{5+}/V^{4+} couples are both pinned at the top of the S 3p bands.[79]

Since only one Li can be removed from a layered oxide and the nickel redox couples are both accessible in the presence of Mn^{4+}, it was logical to investigate the oxides $Li(Ni_{0.25-y}Mn_{0.75-z}Li_{y+z})O_2$[88,89] that are more easily prepared with the Li well-ordered into the Li layers. Lu and Dahn[88] extracted Li from nominal $Li_{1-x}(Ni_{0.25}Li_{0.167}Mn_{0.583})O_2$ to obtain the voltage profile of the second panel of Figure 15; we compare it with that for $Li_{1-x}(V_{0.25}Cr_{0.75})S_2$. At $x = 0.5$, the Ni^{4+} valence is reached in the oxide, the V^{5+} valence is reached in the sulfide. In each, the voltage profile is flat for $0.5 < x < 1$ where the Fermi energy falls below the pinned redox couple of antibonding states at the top of the anion p bands; see Figure 17. A flat $V = 4.5$ V places the Fermi energy above the HOMO of the electrolyte, which we estimated to be at $V \approx 4.75$ V. This observation means that the flat voltage profile signals the voltage limit has been reached, i.e. an E_F in the O 2p band, rather than an oxidation of the electrolyte. This situation must surely be the case in the sulfide. At the intrinsic voltage limit, a second phase appears in the electrode. Once the second phase has been segregated in the oxide on the initial charge, the electrode cycles with a reduced capacity in the majority phase. In the sulfide, formation of the second phase appears to be more reversible as if initially disulfide ions are created on the surface before segregation of $Li_2S + Cr_2S_3$. Similarly, some peroxide ions may form reversibly on the oxide before segregation of Li_2O and MnO_2.

The third panel of Figure 15 shows that on further decrease of the Ni concentration and increase of the Mn concentration in nominal $Li_{1-x}(Ni_{0.17}Li_{0.22}Mn_{0.61})O_2$, the onset of the flat $V = 4.5$ is introduced at a smaller x with a subsequent reversible capacity similar to that of $Li_{1-x}(Ni_{0.25}Li_{0.167}Mn_{0.583})O_2$ whereas $Li_{1-x}(V_{0.1}Cr_{0.9})S_2$ exhibits an initial capacity fade that becomes reversible with a reduced capacity after several cycles. These observations are consistent with the coexistence of two phases in the electrode where the voltage becomes flat with a reversible cycling once the second phase is segregated out.

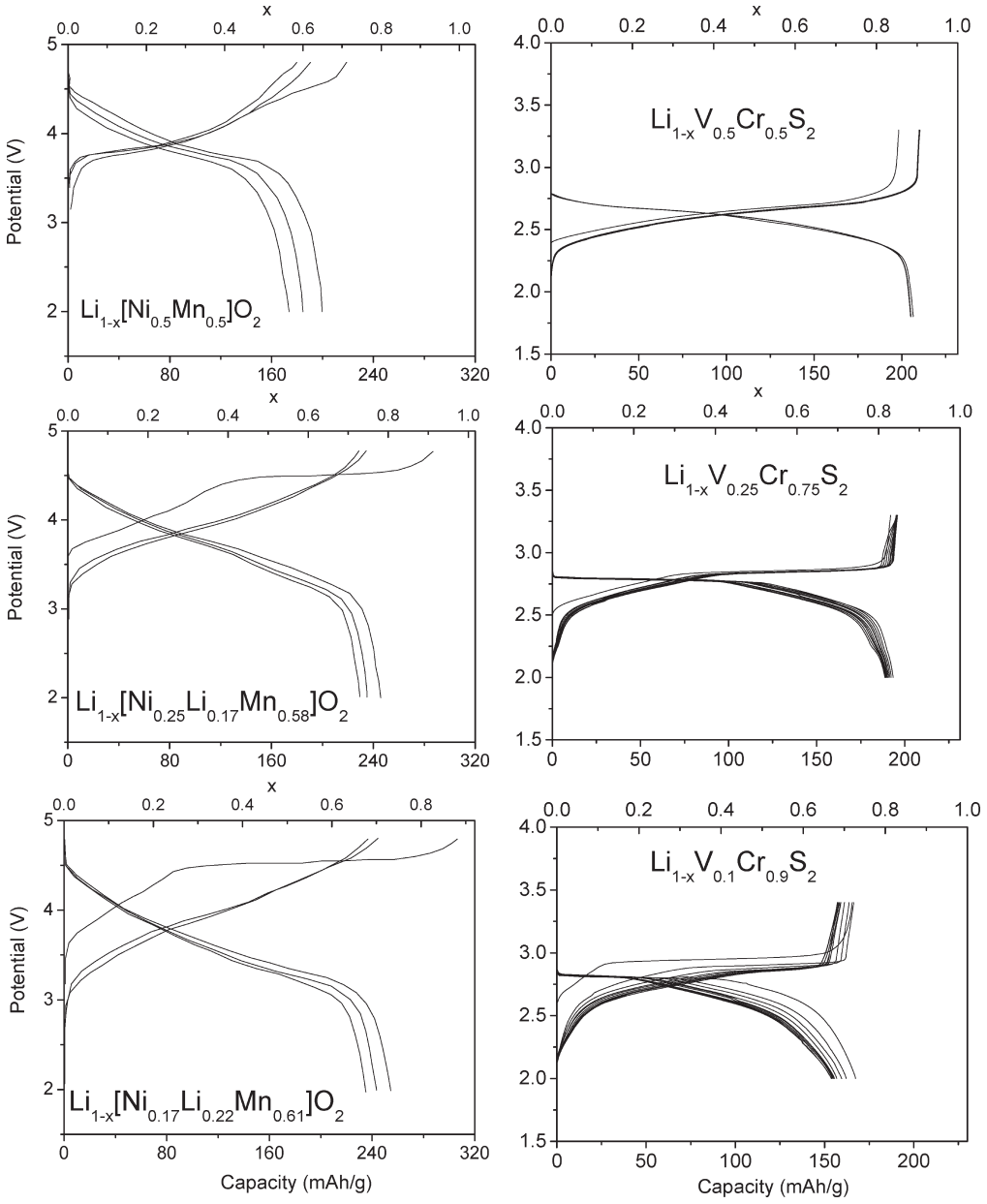

Figure 15. Voltage profiles for the charge and discharge curves on cycling of Li intercalation into $Li_{1-x}[Ni_yLi_{(1/3-2y/3)}Mn_{(2/3-y/3)}]O_2$ and $Li_{1-x}[V_yCr_{1-y}]S_2$, respectively. The flat voltage curves at 4.5 and 2.8 V indicate intrinsic voltage limits for the layered oxide and layered sulfide. Adapted from refs 89 and 79.

Indeed, Thackeray et al.[90] have argued that the attempt to introduce excess Li homogeneously into the transition-metal layers does not occur; but a coexistence of $Li_2MnO_3 = Li(Li_{0.33}Mn_{0.67})O_2$ layers is interleaved with $Li(Ni_{0.5-y}Mn_{0.5+y})O_2$ layers with the transformation

$$Li_2MnO_3 = Li_2O + MnO_2 \quad (3)$$

occurring at $V = 4.5$ V.

Cathode SEI Layers. Extensive research has been devoted to characterization of the SEI layer formed on lithium and on carbon anodes by reduction of the electrolyte $LiPF_6$ in EC/DEC;[8,63] this amorphous Li-electrolyte layer is complex, and the rate at which it is healed after it is broken by changes in the electrode volume on charge and discharge is difficult to measure accurately. Preliminary work[52,53] on the SEI layers formed on oxide cathodes by an oxidative reaction of the electrode with the carbonate electrolyte indicates that these SEI layers are generally unstable; the electrolyte is not protected from further oxidation on subsequent cycling. A continued electrode−electrolyte reaction on cycling thickens the SEI layer, and progressive fading of the reversible capacity of the cathode is related to the thickening of the SEI layer. Moreover, ambiguity in the measurement of the onset of the oxidation reaction has given a reported HOMO of the electrolyte $LiPF_6$ in EC/DEC located at 4.5 ± 0.2 eV versus Li^+/Li^0. This ambiguity may be enhanced by a dependence of the oxidation voltage on the SEI product, which can vary from one electrode material to another. However, confusion between the intrinsic voltage limit of an electrode and the HOMO voltage may also contribute to this ambiguity.

Attempts to create a stable SEI passivation layer on an oxide cathode have used two approaches: one seeks to

identify an additive[91] to the electrolyte such as the EC component for the carbon anode; the other attempts to coat the cathode particles with a main-group oxide that is permeable to Li^+ ions.[92] The former approach forms the SEI layer in situ after the electrode particles have made contact with the carbon of the particle/carbon composite electrode, so the SEI layer formed does not interfere with electronic contact between particles and the current collector. The second approach has obtained some improvement in cyclability, but complete coverage of the active particles with a passivation layer before fabricating the particle/carbon composite electrode would seem to inhibit electronic contact with the current collector. How to coat the cathode/electrolyte interface with a stable SEI layer while retaining electronic contact with the current collector is a continuing challenge for cathodes that would provide a $V > 4.8$ V versus Li^+/Li^0 in the electrolyte $LiPF_6$ in EC/DEC.

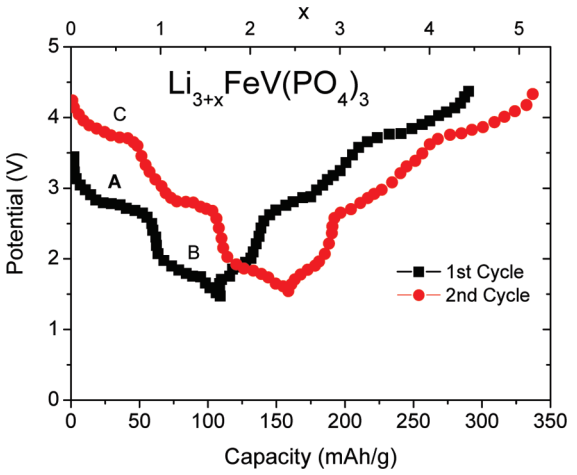

Figure 16. Voltage steps in the NASICON structure of $Li_3FeV(PO_4)_3$. Plateau A of the first discharge corresponds to the Fe^{3+}/Fe^{2+} redox couple at 2.8 V; plateau B to the V^{3+}/V^{2+} redox couple at 1.7 V; plateau C in the second discharge to the V^{4+}/V^{3+} redox couple at 3.7 V. Adapted from ref 87.

Capacity. The energy density of the cell of a rechargeable battery is the product of the voltage V and the capacity Λ of reversible charge transfer per unit weight in amp hours per gram between the anode and the cathode. The capacity of each electrode may be measured separately versus Li^+/Li^0 in a half-call with Li^0 as the anode. Three types of reversible electrode reactions have been considered: (1) Li insertion into a transition-metal oxide or sulfide host, (2) Li insertion into elements, and (3) Li displacement reactions.

Transition-Metal Oxide or Sulfide Hosts. A transition-metal oxide or sulfide host may be a layered compound or a framework structure with 1D, 2D, or 3D interconnected interstitial space for the guest Li atoms. Several examples have been discussed above. The voltage given by the host electrode was seen to be the energy of the operative transition-metal redox couple. A flat voltage profile versus Li concentration is preferred; it is found where two phases coexist rather than where there is a solid solution between the charged and discharged host. With this strategy, the capacity is generally restricted to no more than one Li per transition-metal atom; but where the redox couple of a transition-metal atom is pinned at the top of an anion p band, two redox couples per that transition-metal ion may be accessed. This situation was illustrated by the Ni in $Li_{1-x}(Ni_{0.5}Mn_{0.5})O_2$ and by V in $Li_{1-x}(V_{0.5}Cr_{0.5})S_2$. However, as these examples illustrate, it is not possible to take advantage of this accessibility unless the host can accommodate more than one Li per transition-metal atom without a voltage step. Framework structures with a large interstitial space are needed to obtain a capacity of more than one Li per transition-metal

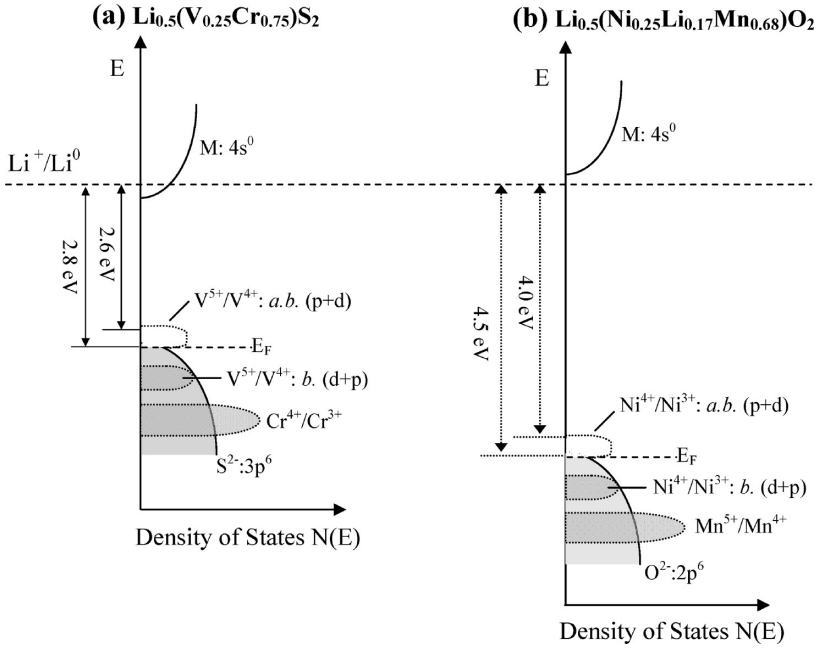

Figure 17. (a) Positions of the M^{n+1}/M^n redox couples relative to the Fermi energy of lithium in (a) $Li_{0.5}(V_{0.25}Cr_{0.75})S_2$ and (b) $Li_{0.5}(Ni_{0.25}Li_{0.17}Mn_{0.68})O_2$; 2.8 eV in the layered sulfide and 4.5 eV in the layered oxide correspond to the flat curves in their voltage profiles in Figure 15.

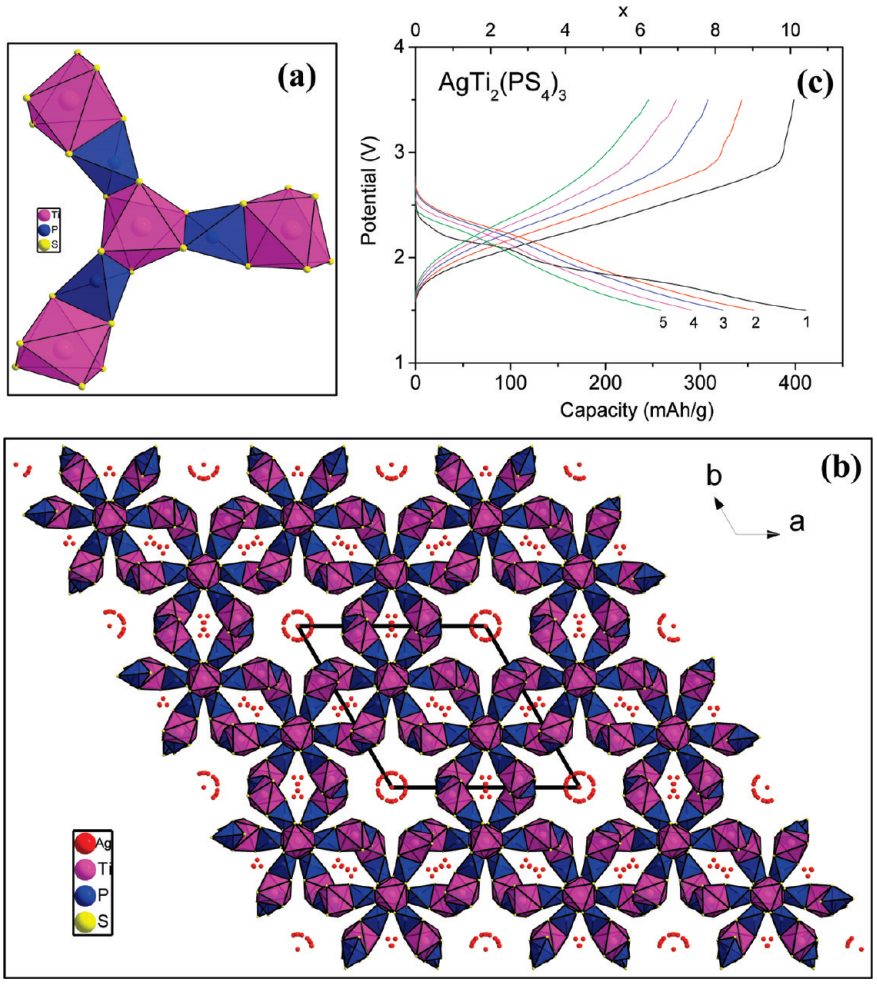

Figure 18. (a) Structural units and (b) projection in the $a-b$ plane for $AgTi_2(PS_4)_3$. (c) Discharge and charge curves for $AgTi_2(PS_4)_3$ over five cycles at (a) 1.5−3.5 V at 0.1 mA/cm^2. Reprinted with permission from refs 93 (Copyright 2008 American Chemical Society) and 94 (Copyright 2008 Elsevier).

atom, but such frameworks tend to be unstable if the large cations that they form around are replaced by smaller Li^+ ions. On the other hand, the NASICON $M_2(XO_4)_3$ framework is capable of receiving reversibly up to 5 Li atoms and the $M_2(PS_4)_3$ framework of $AgTi_2(PS_4)_3$ illustrated in Figure 18 has been shown[93,94] to accommodate up to 10 Li atoms; but, reduction of the PS_4 groups as well as the Ti^{4+} to Ti^0 destabilizes the framework. Moreover, the host must be stable in the electrolyte; $LiV_2(PS_4)_3$ dissolves in the electrolyte $LiPF_6$ in EC/DEC.

Element Hosts. Any element as host intended for use as an anode gives a voltage less than the voltage of the LUMO of a carbonate electrolyte. Therefore, a passivating SEI layer must protect such an anode against chemical reaction with the electrolyte. The most successful elemental host is carbon. Graphite has a layered structure with three strong bonds in the graphite planes and half-filled p_z orbitals perpendicular to the planes that can interact with the Li 2s orbitals. This bonding arrangement limits the volume expansion on Li insertion, but also the number of Li atoms that can be accommodated. Although graphite can only accept one Li per six C atoms, the capacity is still large, the volume expansion is manageable, and its voltage changes little with the Li content. The situation is similar with disordered carbon. Moreover, the EC component and VC additive of a DEC or DMC electrolyte creates a passivating SEI layer on carbon that is healed quickly when cracked by the volume expansion of the carbon mass on Li insertion. Nevertheless, the rate of Li^+-ion transfer across the SEI layer and/or the rate of healing of the SEI layer limits the safe rate of recharging of a carbon anode. Safety concerns associated with plating of Li on the surface of the anode and subsequent dendrite formation require a design of large-scale power batteries using carbon anodes that protects against failure of an individual cell.

More Li can be inserted into Si than into C, which makes it potentially an anode of exceptionally high capacity, but a volume expansion of over 300% on full charge is not manageable. Although the fabrication of nanowires has been touted as a solution to this problem,[95,96] this anode suffers from continuing formation of an SEI layer that does not protect against interaction with the electrolyte. Similar problems are encountered with Li replacements for H in metal hydrides.

Displacement Reactions. Displacement of an element from a compound or an alloy can be reversible,[97,98] as was first demonstrated with the displacement of iron from Fe_3O_4 on insertion of more than one Li per formula unit.[99] Exploitation of this phenomenon promised a large

capacity since a displacement may involve reducing the displaced atom by more than one electron.[100,101] These reactions are of particular interest for anodes with main-group atoms; they offer voltages less than the voltage of the LUMO of a carbonate electrolyte. However, this strategy suffers from large volume changes in a charge/discharge cycle and the need for a stable passivating layer that can heal more quickly than reaction with the bulk electrolyte or the excess Li^+ ions at the surface. This approach is only promising if the LUMO of the electrolyte can be raised above the μ_A of the anode. Nevertheless, amorphous Si or displacement reactions that are buffered with graphite can improve the capacity of a carbon anode.

Summary

The principal challenges facing the development of batteries for electric vehicles are cost, safety, cell energy density (voltage × capacity), rate of charge/discharge, and service life. Automation of manufacturing, material selection, and service life are the keys to lower costs; the availability of Li need not be a problem. Long service life requires elimination of unwanted chemical reactions between the electrodes and the electrolyte as well as retention over many charge/discharge cycles of the electronic contact between the active particles of an electrode and the current collector. The latter requirement restricts the volume change versus state of charge that can be tolerated in an electrode unless the active electrode particles are tethered to a current collector. This attachment may be made directly by the growth of nanowires of active material on a current-collector substrate; it may also be done by bonding the active particles to a conductive polymer having a conduction band that overlaps the μ_A or μ_C of the electrode. The former rate is being researched with Si nanowires,[95] the latter has been accomplished with polypyrrole bonded to carbon-coated $LiFePO_4$.[102,103]

Safety is related to the flammability of the electrolyte, the rate of charge and/or discharge, and the engineering of the battery pack. A hybrid ionic liquid and organic liquid as the electrolyte solvent can be made nonflammable without too great a compromise of the electrolyte σ_{Li}. Both the $LiFePO_4$ cathode and the $Li_4Ti_5O_{12}$ anode have demonstrated safe and rapid charge and discharge over many cycles where the μ_C and μ_A, respectively, are located within the window of the electrolyte, which removes the requirement of a passivating layer. However, location of the μ_C and μ_A within the electrolyte window is not sufficient if the electrode is operating at its voltage limit with a redox couple pinned to the top of an anion p band or overlapping a cation 4s band. An electrolyte with a larger window, especially one with a higher LUMO, would be helpful; but EC and/or VC in the electrolyte solvent do allow use of a carbon anode with a limited charging rate. Finally, engineering the battery-pack design to allow failure of one cell without compromising the entire stack can also build in safety.

A greater energy density requires both a larger voltage and larger capacity. To achieve a greater energy density with inexpensive electrodes having a long service life is a challenge for the materials scientist. On the anode side, it will be difficult to have a better capacity than that of carbon, and the passivation layer makes it possible to take advantage of a μ_A above the LUMO of the electrolyte, albeit at the expense of a reduced charging rate. On the cathode side, a material having a redox couple pinned at the top of the O 2p band, but with two valence states accessible without exceeding the intrinsic voltage limit of the oxide, would offer the maximum voltage and capacity. The upper intrinsic voltage limit of such an oxide can be raised by increasing the covalent component of the M−O bond of a countercation to lower the energy E_V of the top of the O 2p bands; but this tuning of E_V must not also push the pinned redox couple further than the change in E_V. Comparison of the upper voltage limits of the nickel oxides having Li in octahedral versus tetrahedral sites illustrates a tuning of E_V by 1.0 V. However, to take advantage of the availability of two redox couples on a single transition-metal atom, it is necessary to have a host structure that can accept two Li atoms per transition-metal cation. Can nature and/or the imagination of the solid state chemist identify such an electrode material with a μ_C matched to the electrolyte window? An example of the imaginative materials design that may be needed is given by a recent report from Sun et al.[104]

Acknowledgment. This work was supported by the office of FreedomCAR and Vehicle Technologies of the U.S. Department of Energy under contract no. DE-AC03-76SF00098 and the Robert A. Welch Foundation of Houston, TX (Grant No. F-1066).

References

(1) http://www.eia.doe.gov/fuelrenewable.html. Accessed on 05/25/2009.
(2) http://www.greencarbongress.com. Accessed on 05/25/2009.
(3) Hayashi, K.; Nemoto, Y.; Tobishima, S.; Yamaki, J. *Electrochim. Acta* **1999**, *44*, 2337.
(4) Xu, K. *Chem. Rev.* **2004**, *104*, 4303.
(5) Imhof, R.; Novak, P. *J. Electrochem. Soc.* **1999**, *146*, 1702.
(6) Egashira, M.; Takahashi, H.; Okada, S.; Yamaki, J. *J. Power Sources* **2001**, *92*, 267.
(7) Zhang, X.; Kostecki, R.; Richardson, T. J.; Pugh, J. K.; Ross, P. N. *J. Electrochem. Soc.* **2001**, *148*, A1341.
(8) Fong, R.; van Sacken, U.; Dahn, J. R. *J. Electrochem. Soc.* **1990**, *137*, 2009.
(9) Yazami, R. *Electrochim. Acta* **1999**, *45*, 87.
(10) Vogdanis, L.; Martens, B.; Uchtmann, H.; Hensel, F.; Heitz, W. *Makromolekul. Chem.* **1990**, *191*, 465.
(11) Sloop, S. E.; Pugh, J. K.; Wang, S.; Kerr, J. B.; Kinoshita, K. *Electrochem. Solid-State Lett.* **2001**, *4*, A42.
(12) Smart, M. C.; Smith, K. A.; Bugga, R. V.; Whitcanack, L. D. In *Electrolytes for Wide Operating Temperature Range Li-Ion Cells*. 4th Annual International Conference: Lithium Mobile Power 2008, Las Vegas, NV, December 8−9, 2008.
(13) Koch, V. R.; Dominey, L. A.; Nanjundiah, C.; Onderchen, M. J. *J. Electrochem. Soc.* **1996**, *143*, 798.
(14) Webber, A.; Blomgren, G. E. In *Advances in Li-Ion Batteries*; van Schalkwijk, W., Scrosati, B., Eds.; Kluwer Academic/Plenum Publishers: New York, 2002; Chapter 6.
(15) Garcia, B.; Lavallee, S.; Perron, G.; Michot, C.; Armand, M. *Electrochim. Acta* **2004**, *49*, 4583.
(16) Markevich, E.; Baranchugov, V.; Aurbach, D. *Electrochem. Commun.* **2006**, *8*, 1331.
(17) Wang, Y.; Zaghib, K.; Guerfi, A.; Bazito, F. F. C.; Torresi, R. M.; Dahn, J. R. *Electrochim. Acta* **2007**, *52*, 6346.
(18) Fuller, J.; Carlin, R. T.; Osteryoung, R. A. *J. Electrochem. Soc.* **1997**, *144*, 3881.
(19) Zaghib, K. personal communication.
(20) Stassen, I.; Hambitzer, G. *J. Power Sources* **2002**, *105*, 145.

(21) Zinck, L.; Borck, M.; Ripp, C.; Hambitzer, G. *J. Appl. Electrochem.* **2006**, *36*, 1291.
(22) Wright, P. V. *Brit. Polym. J.* **1975**, *7*, 319.
(23) Armand, M. B.; Chagbano, J. M.; Duclot, M. J. In *Fast Ion Transport in Solid*; Vashishta, P., Mundy, J. N., Shenoy, G. K., Eds.; Elsevier N Holland: New York, 1979; p131.
(24) Nishimoto, A.; Watanabe, M.; Ikeda, Y.; Kojiya, S. *Electrochim. Acta* **1998**, *43*, 1177.
(25) Croce, F.; Appetecchi, G. B.; Persi, L.; Scrosati, B. *Nature* **1998**, *394*, 456.
(26) Croce, F.; Curini, R.; Martinelli, A.; Persi, L.; Ronci, F.; Scrosati, B. *J. Phys. Chem. B* **1999**, *103*, 10632.
(27) Croce, F.; Settimi, L.; Scrosati, B. *Electrochem. Commun.* **2006**, *8*, 364.
(28) Pradel, A.; Ribes, M. *Mater. Chem. Phys.* **1989**, *23*, 121.
(29) Adachi, G.; Imanaka, N.; Aono, H. *Adv. Mater.* **1996**, *8*, 127.
(30) Minami, T.; Hayashi, A.; Tatsumisago, M. *Solid State Ionics* **2006**, *177*, 2715.
(31) Kim, Y.; Saienga, J.; Martin, S. W. *J. Phys. Chem. B* **2006**, *110*, 16318.
(32) Dudney, N. J. In *Lithium Batteries*; Nazri, G. A., Pistoia, G., Eds.; Kluwer Academic Publishers: Norwell, MA, 2004; p 623.
(33) Takada, K.; Aotani, N.; Kondo, S. *J. Power Sources* **1993**, *43*, 135.
(34) Machida, N.; Maeda, H.; Peng, H.; Shigematsu, T. *J. Electrochem. Soc.* **2002**, *149*, A688.
(35) Nagata, K.; Nanno, T. *J. Power Sources* **2007**, *174*, 832.
(36) Bates, J. B.; Dudney, N. J.; Neudecker, B.; Ueda, A.; Evans, C. K. *Solid State Ionics* **2000**, *135*, 33.
(37) Feuillade, G.; Perche, Ph. *J. Appl. Electrochem.* **1975**, *5*, 63.
(38) Appetecchi, G. B.; Croce, F.; Marassi, R.; Persi, L.; Romagnoli, P.; Scrosati, B. *Electrochim. Acta* **1999**, *45*, 23.
(39) Persi, L.; Croce, F.; Scrosati, B. *Electrochem. Commun.* **2002**, *4*, 92.
(40) Scrosati, B. In *Advances in Li-Ion Batteries*; van Schalkwijk, W., Scrosati, B., Eds.; Kluwer Academic/Plenum Publishers: New York, 2002; Chapter 8.
(41) Fuller, J.; Breda, A. C.; Carlin, R. T. *J. Electrochem. Soc.* **1997**, *144*, L67.
(42) Shin, J.-H.; Henderson, W. A.; Passerini, S. *Electrochem. Commun.* **2003**, *5*, 1016.
(43) Ye, H.; Huang, J.; Xu, J. J.; Khalfan, A.; Greenbaum, S. G. *J. Electrochem. Soc.* **2007**, *154*, A1048.
(44) Sirisopanaporn, C.; Fernicola, A.; Scrosati, B. *J. Power Sources* **2009**, *186*, 490.
(45) Guerfi, A.; Dontigny, M.; Kobayashi, Y.; Vijh, A.; Zaghib, K. *J. Solid State Electr.* **2009**, *13*, 1003.
(46) Cho, J.; Liu, M. *Electrochim. Acta* **1997**, *42*, 1481.
(47) Hayashi, A.; Kitade, T.; Ikeda, Y.; Kohjiya, S.; Matsuda, A.; Tatsumisago, M.; Minami, T. *Chem. Lett.* **2001**, 814.
(48) Inda, Y.; Katoh, T.; Baba, M. *J. Power Sources* **2007**, *174*, 741.
(49) Murphy, D. W.; Carides, J. N.; DiSalvo, F. J.; Cros, C.; Waszczak, J. V. *Mater. Res. Bull.* **1977**, *12*, 825.
(50) Kim, Y.; Goodenough, J. B. *Electrochem. Solid-State Lett.* **2009**, *12*, A73.
(51) Blyr, A.; Sigala, C.; Amatucci, G.; Guyomard, D.; Chabre, Y.; Tarascon, T. M. *J. Electrochem. Soc.* **1998**, *145*, 194.
(52) Aurbach, D. *J. Power Sources* **2000**, *89*, 206.
(53) Edstrom, K.; Gustafsson, T.; Thomas, J. O. *Electrohim. Acta* **2004**, *50*, 397.
(54) Wang, Z.; Sun, Y.; Chen, L.; Huang, X. *J. Electrochem. Soc.* **2004**, *151*, A914.
(55) Padhi, A. K. Ph.D. Mapping Redox Energies of Electrode Materials for Lithium Batteries. Thesis, The University of Texas at Austin, 1997.
(56) Steele, B. C. H. In *Fast Ion Transport in Solids*; van Gool, W., Ed.; North-Holland: Amsterdam, 1973.
(57) Wittingham, M. S. *Science* **1976**, *192*, 1126.
(58) Mitzushima, K.; Jones, P. C.; Wiseman, P. J.; Goodenough, J. B. *Mater. Res. Bull.* **1980**, *15*, 783.
(59) Wittingham, M. S. In *Fast Ion Transport in Solids*; van Gool, W., Ed; North-Holland: Amsterdam, 1973.
(60) Dampier, F. W. *J. Electrochem. Soc.* **1974**, *121*, 656.
(61) Goodenough, J. B.; Mizushima, K.; Takeda, T. *Jpn. J. Appl. Phys.* **1980**, *19*−*3*, 305.
(62) Dey, A. N.; Sullivan, B. P. *J. Electrochem. Soc.* **1970**, *117*, 222.
(63) Aurbach, D, In *Advances in Li-Ion Batteries*; van Schalkwijk, W., Scrosati, B., Eds.; Kluwer Academic/Plenum Publishers: New York, 2002; Chapter 1.
(64) Nagaura, T.; Tozawa, K. *Prog. Batteries Solar Cells* **1990**, *9*, 209.
(65) Sinha, S.; Murphy, D. W. *Solid State Ionics* **1986**, *20*, 81.
(66) Thackeray, M. M.; David, W. I. F.; Bruce, P. G.; Goodenough, J. B. *Mater. Res. Bull.* **1983**, *18*, 461.
(67) Thackeray, M. M.; Jahnson, P. J.; De Picciotto, L. A.; Bruce, P. G.; Goodenough, J. B. *Mater. Res. Bull.* **1984**, *19*, 435.
(68) Amatucci, G. G.; Pereira, N; Zheng, T.; Tarascon, J.-M. *J. Electrochem. Soc.* **2001**, *148*, A171.
(69) Choi, W.; Manthiram, A. *J. Electrochem. Soc.* **2007**, *154*, A792.
(70) Goodenough, J. B.; Hong, H.Y.-P.; Kafalas, J. A. *Mater. Res. Bull.* **1976**, *11*, 203.
(71) Manthiram, A.; Goodenough, J. B. *J. Solid State Chem.* **1987**, *71*, 349.
(72) Goodenough, J. B. *Electrochem. Soc. Proc.* **2000**, *99-24*, 1.
(73) Goodenough, J. B. In *Advances in Li-Ion Batteries*; van Schalkwijk, W., Scrosati, B., Eds.; Kluwer Academic/Plenum Publishers: New York, 2002; Chapter 4.
(74) Padhi, A. K.; Nanjundaswamy, K. S.; Goodenough, J. B. *J. Electrochem. Soc.* **1997**, *144*, 1188.
(75) Johnston, D. C.; Prakash, H.; Zachariasen, W. H.; Viswanathan, R. *Mater. Res. Bull.* **1973**, *8*, 777.
(76) Edwards, P. P.; Egdell, R. G.; Fragala, I.; Goodenough, J. B.; Harrison, M. R.; Orchard, A. F.; Scott, E. G. *J. Solid State Chem.* **1984**, *54*, 127.
(77) Harrison, M. R.; Edwards, P. P.; Goodenough, J. B. *J. Solid State Chem.* **1984**, *54*, 426.
(78) Ferg, E.; Gummow, R. J.; de Kock, A.; Thackeray, M. M. *J. Electrochem. Soc.* **1994**, *141*, L147.
(79) Goodenough, J. B.; Kim, Y. J. *Solid State Chem.*, in press.
(80) Hert, J. T.; Huang, Q; McQueen, T.; Klimczuk, T.; Bos, J. W. G.; Viciu, L.; Cava, R. J. *Phys. Rev. B* **2008**, *77*, 075119.
(81) Kim, Y.; Goodenough, J. B. *J. Phys. Chem. C* **2008**, *112*, 15060.
(82) Kim, Y.; Park, K. S.; Song, S. H.; Han, J. T.; Goodenough, J. B. *J. Electrochem. Soc.* **2009**, *156*, A703.
(83) Jellinek, F. *Acta Crystallogr.* **1957**, *10*, 620.
(84) Kim, J.-H.; Myung, S.-T.; Yoon, C. S.; Oh, I.-H.; Sun, Y.-K. *J. Electrochem. Soc.* **2004**, *151*, A1911.
(85) Schougaard, S. B.; Breger, J.; Jiang, M.; Grey, C. P.; Goodenough, J. B. *Adv. Mater.* **2006**, *18*, 905.
(86) Kang, K.; Carlier, D.; Reed, J.; Arroyo, E. M.; Ceder, G.; Croguennec, L.; Delmas, C. *Chem. Mater.* **2003**, *15*, 4503.
(87) Nanjundaswamy, K. S.; Padhi, A. K.; Goodenough, J. B.; Okada, S.; Ohtsuka, H.; Arai, H.; Yamaki, J. *Solid State Ionics* **1996**, *92*, 1.
(88) Lu, Z.; Dahn, J. R. *J. Electrochem. Soc.* **2002**, *149*, A815.
(89) Park, Y. J.; Hong, Y. S.; Wu, X. W.; Ryu, K. S.; Chang, S. H. *J. Power Sources* **2004**, *129*, 288.
(90) Thackeray, M. M.; Kang, S. H.; Johnson, C. S.; Vaughey, J. T.; Benedek, R.; Hackney, S. A. *J. Mater. Chem.* **2007**, *17*, 3112.
(91) Abe, K.; Ushigoe, Y.; Yoshitake, H.; Yoshio, M. *J. Power Sources* **2006**, *153*, 328.
(92) Liu, J.; Manthiram, A. *Chem. Mater.* **2009**, *21*, 1695.
(93) Kim, Y.; Arumugam, N.; Goodenough, J. B. *Chem. Mater.* **2008**, *20*, 470.
(94) Kim, Y.; Goodenough, J. B. *Electrochem. Commun.* **2008**, *10*, 497.
(95) Chan, C. K.; Peng, H.; Liu, G.; Mcllwrath, K.; Zhang, X. F.; Huggins, R.; Cui, Y. *Nat. Nanotechnol.* **2008**, *3*, 31.
(96) Kim, H.; Cho, J. *Nano Lett.* **2008**, *8*, 3688.
(97) Arico, A. S.; Bruce, P.; Scrosati, B.; Tarascon, J.-M.; Schalkwijk, W. V. *Nat. Mater.* **2005**, *4*, 366.
(98) Bruce, P. G.; Scrosati, B.; Tarascon, J.-M. *Angew. Chem., Int. Ed.* **2008**, *47*, 2930.
(99) Thackeray, M. M.; David, W. I. F.; Goodenough, J. B. *Mater. Res. Bull.* **1982**, *17*, 785.
(100) Thackeray, M. M.; Vaughey, J. T.; Johnson, C. S.; Kropf, A. J.; Tostmann, H.; Benedek, R.; Sarankonsri, T.; Hackney, S. A. *Proc.*−*Electrochem. Soc.* **2001**, *2000*−*36*, 92.
(101) Thackeray, M. M.; Vaughey, J. T.; Fransson, L. M. L. *JOM* **2002**, *54*, 20.
(102) Park, K. S.; Schougaard, S. B.; Goodenough, J. B. *Adv. Mater.* **2007**, *19*, 848.
(103) Huang, Y. H.; Park, K. S.; Goodenough, J. B. *J. Electrochem. Soc.* **2006**, *153*, A2282.
(104) Sun, Y.-K.; Myung, S.-T.; Park, B.-C.; Prakash, J.; Belharouak, I.; Amine, K. *Nat. Mater.* **2009**, *8*, 320.